MEASUREMENT OF THE RATE COEFFICIENTS FOR THE BIMOLECULAR AND TERMOLECULAR CHARGE TRANSFER REACTIONS OF He_2^+ WITH Ne, Ar, N_2, CO, CO_2, AND CH_4

DISSERTATION

Presented to the Graduate Council of the North Texas State University in Partial Fulfillment of the Requirements

For the Degree of

DOCTOR OF PHILOSOPHY

By

Francis Wha-Pyo Lee, B.S., M.S.

Denton, Texas

May, 1977

Lee, Francis Wha-pyo, Measurement of the Rate Coefficients for the Bimolecular and Termolecular Charge Transfer Reactions of He_2^+ with Ne, Ar, N_2, CO, CO_2, and CH_4. Doctor of Philosophy (Physics), May, 1977, 111 pp., 3 tables, 32 illustrations, bibliography, 41 titles.

The problem with which this investigation is concerned is that of measuring the rate coefficients for termolecular charge transfer reactions of He_2^+ in atmospheric pressure afterglows with the minority reacting species.

The concept of the rate coefficients for the bimolecular and termolecular charge transfer reactions of He_2^+ with the secondary reacting species, theory of charge transfer process, and the reaction processes affecting the He_2^+ population in a pure helium plasma have been reviewed in detail. The equipment and the experimental techniques have been described.

In particular the measurements of termolecular charge transfer reactions into non-associative product channels were described. Ion destruction frequencies have been experimentally determined from the selectively excited fluorescence of N_2^+ in high pressure afterglows of mixed gases excited by an intense electron beam discharge. Data have been obtained as functions of helium pressure over the range from 300 to 1500 torr and as functions of the partial pressure

of reactant from 25 to 400 μ Hg. From these data, pressure dependent rate coefficients have been extracted and subsequently resolved into contributions from bimolecular and termolecular components for reactions of He_2^+ with Ne, Ar, N_2, CO, CO_2, and CH_4. The bimolecular components have been found to agree with the results shown in literatures to within experimental error, and in some cases the values reported here represent an improvement in precision.

Of particular interest was the discovery that the presence of a third body can change an improbable charge transfer reaction involving He_2^+ into a very probable one, as in the case of the reaction with argon. For example, in Tables II and II it was shown that less than a 300 torr pressure of helium was required to double the effective rate of reaction of argon with He_2^+ while over 3000 torr was required for CH_4.

The sensitivity of the method has been sufficient to detect termolecular components as small as 2×10^{-30} cm^6/sec and values were found to range widely from 2×10^{-30} for Ne to 67×10^{-30} cm^6/sec for CO_2. The size of these termolecular rates not only served to explain specific anomalous efficiencies of the charge transfer process observed in atmospheric pressure lasers but also suggested the general importance of three-body ion-molecule reactions in higher pressure plasmas.

TABLE OF CONTENTS

LIST OF TABLES

LIST OF ILLUSTRATIONS

CHAPTER I

INTRODUCTION

The majority of kinetic investigations in gases are carried out with the objective of gaining insight into the mechanisms by which reactions occur. These investigations may be solely concerned with establishing the reaction mechanism in a particular system, or if that is known, studies of the reaction kinetics may be concerned with the details of the rates of the interaction of the reactants. When the reactions of interest involve atomic and molecular species with very short characteristic lifetimes, studies are typically conducted in gaseous plasmas in which the reactive species may be produced as fragments of energetic collisions, often with electrons. In particular the studies of reactions involving ions of small molecules in the gas phase fall into this category and the literature is rich in examples of this type of work.

Although such reactions of ions are of fundamental importance to chemistry, until recent times, their study had received its greatest motivation from applications in ionospheric physics. As a result, studies of reactions involving atmospheric ions have received much attention

and a rather profound understanding of these processes has developed. Conversely, the reactions of ions of little importance to earthlike or planetary atmospheres have received proportionally less attention. Only recently have the successes in using charge transfer mechanisms to pump high-energy lasers refocussed interest onto the reactions of non-atmospheric ions. It is the study and quantitative measurement of the characteristic rates of reactions for one such ion, He_2^+, that is the subject of the work reported here.

In 1947, Bates and Massey[1] initiated the modern interest in charge transfer reactions by suggesting that atomic ions such as O^+, produced in the upper atmosphere of the earth through photoionization of O_2 (or O) by solar ultraviolet radiation, might be interacting with other neutral atoms and molecules by charge transfer. In general it was found that the loss of the photoions follows the pattern that charge transfer reactions convert the primary ions to species which can be more readily lost by recombination than could the original atomic ions. For example, in the region near 300 Km where the dominant ion is O^+, the reactions,

$$O^+ + N_2 \rightarrow NO^+ + N \qquad (1.1)$$

$$O^+ + O_2 \rightarrow O_2^+ + O \qquad (1.2)$$

are considered important in converting the primary ion, O^+, to molecular species, NO^+ and O_2^+, which may then recombine by dissociative recombination,

$$NO^+ + e \rightarrow N + O \quad , \tag{1.3}$$

$$O_2^+ + e \rightarrow O + O \quad . \tag{1.4}$$

This tends to control the electron density[2] in the ionosphere. Although most of these types of ion-neutral reactions have been studied in laboratory plasmas, there have been some difficulties in producing a laboratory plasma with properties similar to the ionosphere. In situ measurements using rockets and satellites have attempted to use the ionosphere itself as the "laboratory plasma" and many useful results have been achieved.

More recently, however, drift tube techniques have been widely applied in the study of ion-molecule reactions. This technique introduced the major technical development of mass spectrometric sampling of the reacting ions. As implemented, this generally occurred at the end of the flight path through a drift tube in which the number of collisions that the ion underwent with molecules during its travel could be varied over a wide range. However, one of the most productive methods used in kinetic investigations of the reactions involving ions has been the study of the behavior with time of the afterglows of electric discharges

in a gaseous media. Such afterglows may be considered to be the plasmas existing during the periods of time extending from the cessation of sources of excitation of gaseous discharges to the time when the ionization densities go essentially to zero. Observations of the evolution of the populations of various ionic reactants and products in suitable afterglows have been used in the study of the reactions of both atmospheric and non-atmospheric ions. Although the reactivity of inert gas molecular ions was first suggested by data obtained in an active discharge, virtually all of the subsequent work demonstrating the general importance of the reactivity was done with such afterglow systems. It is with the reactivity of one inert gas molecular ion, He_2^+, that this work is concerned.

In 1957 Oskam[3] first suggested, from the study of the segregation in a discharge of a very small neon impurity in helium, that the ions of inert gas molecules might be significantly reactive. He postulated that the preferential production of neon ions in helium afterglows might be occurring as a result of the process,

$$He_2^+ + Ne \rightarrow Ne^+ + 2He \quad , \qquad (1.5)$$

as was independently verified by Loeb[4] and Pahl and Weimer.[5] In collaboration with Mittelstadt,[6] Oskam reported the estimation of a relatively large binary reaction rate,

$1.5 \times 10^{-10} cm^3/sec$, for the reaction (1.5). They determined this rate by measuring the spatial gradients of the electron density in a stationary microwave afterglow in which the gas was spatially fixed. However, this technique has not been utilized very widely for other quantitative rate measurements since the mobilities for most ions do not vary widely and competing reactions can cause confusion.

The development of ion-molecule reaction studies has been more strongly influenced by the introduction of the flowing afterglow technique. This technique differs from that of the stationary afterglow in substituting space resolution for time resolution. Thus, the composition of the afterglow can be controlled in space in a way that is not possible in time. In 1963 Collins and Robertson[7,8,9] first demonstrated spectroscopically that the reactions such as (1.5) could occur more generally with neutral molecules. They reported the selective pumping of emission bands from the reaction products by using a flowing afterglow technique and formulated the reaction mechanisms,[9]

$$He_2^+ + N_2 \rightarrow (N_2^+)^* + 2He \qquad (1.6a)$$

$$He_2^+ + O_2 \rightarrow (O_2^+)^* + 2He \qquad (1.6b)$$

$$He_2^+ + CO \rightarrow (CO^+)^* + 2He \qquad (1.6c)$$

where the asterisk indicates electronic excitation to a radiating state of the product ion. Most of the bimolecular

charge transfer rates important to aeronomy and related studies of planetary atmospheres were subsequently measured to a satisfactory degree of precision[2] with the more general flowing afterglow technique which was developed by the ESSA group.

In 1966, Fehsenfeld, et al.,[10] made the first quantitative measurement of an inert gas molecular ion involved in an ion-molecule reaction such as reactions (1.5) and (1.6a). Though of no importance to aeronomy, they did this in the course of a series of measurements designed for the reactions of helium atomic ions, He^+, with N_2, O_2, H_2, NO, Ne, Ar, CO and CO_2. They reported a rate coefficient for reaction (1.5) with He_2^+ of $1.4 \times 10^{-10} cm^3/sec$ and a rate coefficient for reaction (1.6a) of $6 \times 10^{-10} cm^3/sec$, a value approaching half the theoretical maximum given by the Langevin cross section.[11] Their measurement was made by determining the dependence upon reactant concentration of the He_2^+ concentration measured with a mass spectrometer in low pressure flowing afterglow. In 1968, they modified[12] the flowing afterglow technique to cover a range of gas temperature from 82^o to 600^o K. This was necessary for them to obtain better information about the reaction rate coefficients at ionospheric temperatures, as those were known to vary from somewhat below 300^o K to substantially above 300^o K, depending upon altitude and time. Their investigations of the temperature, or energy, dependence of the rate coefficients

established additional experimental expertise which coincidentally provided an improvement in the production of an afterglow dominated by reactions involving homonuclear inert-gas molecular ions. Previously, charge transfer reactions involving these species had been less tractable to the generally successful flowing afterglow technique for measuring reaction rate coefficient at room temperature because of the experimental difficulties associated with establishing a dominance of the weakly bound molecular ions of the inert gases. In 1970, they[13] finally succeeded in measuring the bimolecular charge transfer rates for He_2^+, Ne_2^+, and Ar_2^+ reacting with Ne, Ar, Kr, NO, O_2, CO_2, N_2 and CO_2 under cryogenic conditions. At temperatures up to 200^o K the necessary predominance of the molecular ions could be established and rates generally approaching the theoretical limit were found. For example, a rate coefficient of $1.3 \times 10^{-9} cm^3/sec$ was reported for reaction (1.6a), which has a value of $1.26 \times 10^{-9} cm^3/sec$ in the theoretical limit. Since a strong dependence on temperature would not be expected, a priori, at least for the highly probable exothermic reactions, the 200^o K values seemed sufficient for existing needs.

Recently the interest in ion-molecule reactions involving inert gas molecules has been refocused by the proposal of Collins, et al.,[14] that resonant charge transfer might

provide a nearly ideal mechanism for pumping high pressure gas lasers. The potential of the pumping sequence,

$$He_2^+ + N_2 \rightarrow N_2^+(B^2\Sigma_u) + 2He \qquad (1.7)$$

was reported in the same letter[14] together with the successful extraction of stimulated emission in the B → X transition,

$$N_2^+(B^2\Sigma_u) + h\nu \rightarrow N_2^+(X^2\Sigma_g) + 2h\nu \quad , \qquad (1.8)$$

in a high pressure helium-nitrogen plasma excited by the discharge of an intense electron beam. The first ion laser pumped by charge transfer from He_2^+ was subsequently constructed[15] and the most recent studies of power output have shown that it is scalable to operation at high power with high efficiency.[16] It appears, a priori, that these mechanisms represent the most efficient means of exploiting, for the production of visible laser radiation, the energy stored in a high pressure gas by an intense electron beam. Moreover, charge transfer offers considerable advantages over other laser pumping mechanisms because of the large cross sections, $10^{-14}cm^2$, characteristic of such processes. These values lead to reaction rates which are at least an order of magnitude larger than those characteristic of most excitation transfer sequences involving neutral atomic and molecular species. Secondary advantages lie in the large

number of possible reaction systems making probable a large selection of transition wavelengths. For example, a weak stimulated emission from CO^+ pumped by an analogous reaction has been observed.[17]

The current attention to these electron-beam lasers has stimulated a further interest in the ion-molecule reactions involving inert gas molecules and partial cross sections for charge transfer from He_2^+ into specific output channels of the reaction have been recently determined in an atomic beam apparatus.[18,19] Nevertheless, in the course of developing this new type of laser, attempts to model the kinetic sequences pumping the high pressure lasers suffered from the paucity of rate coefficient data appropriate to atmospheric pressure. Efforts to describe the strong dependence of laser outputs on gas pressure did not succeed when models were based upon extrapolations of available low pressure data. In the flowing experiments, because of the restricted range of lower operating pressures which were available, the effects of termolecular reaction channels for which the three-body rate coefficient was less than about $3 \times 10^{-28} cm^6/sec$ could not be detected whenever there was a parallel bimolecular channel having a cross section near the Langevin limit.[11] Such a generous limit is not helpful at atmospheric pressures where much smaller termolecular rates would still dominate.

The recent work of Bourène and Lecalvé[20] provided the first suggestion that reaction rate coefficients for He_2^+ measured at high pressures could be significantly different from those derived from low pressure data. In their work, bimolecular rate coefficients for the He_2^+ reactions with O_2, H_2, N_2, CO, CO_2, N_2O, H_2O, CH_4, Ne, Ar, Kr, and Xe at pressure between 50 and 1500 torrs were obtained from the experimental device similar to the one which will be reported here. A comparison with present work is possible in a few cases as shown on Table II in Chapter VI, but no report on termolecular rate coefficient was made in their work.

This work reports what are believed to be the first measurements of termolecular charge transfer reactions into non-associative product channels. These reactions are the termolecular analogs to the well-known[13] bimolecular charge transfer reactions involving helium molecular ions. In a sense they form parallel reaction channels, favored at high pressures, connecting the same reactant and product populations as the bimolecular ion-molecule reactions dominant at low pressures. For example the reaction,

$$He_2^+ + N_2 + He \rightarrow N_2^+(B^2\Sigma_u) + 3He \qquad (1.9)$$

is the termolecular analog of (1.7) and with a rate coefficient of only $10^{-29}cm^3/sec$ it would still dominate in high

pressure lasers operating at several atmospheres while being completely negligible (in comparison with (1.7)) in the conventional low pressure ion-molecule experiments. Evidently, the possibility of termolecular reaction channels paralleling the bimolecular ones has not received much attention in the past and it appears that termolecular channels have been investigated[9] only for associative ion-molecule reactions for which that bimolecular analog is extremely unlikely.

In this work ion destruction frequencies have been determined as functions of helium pressure over the range from 300 to 1500 torr and as functions of the partial pressure of reactant from 25 to 400 μ Hg. From this data pressure-dependent rate coefficients have been extracted and subsequently resolved into contributions from bimolecular and termolecular components for reactions of He_2^+ with Ne, Ar, N_2, CO, CO_2 and CH_4. The bimolecular components have been found to agree with the ESSA results[13] to within experimental error and in some cases the values reported here represent an improvement in precision. The sensitivity of the method has been sufficient to detect termolecular components as small as $2 \times 10^{-30} cm^6/sec$ and values were found to range widely from this threshold value for Ne to $67 \times 10^{-30} cm^6/sec$ for CO_2. The size of these termolecular rates not only serves to explain the anomalous

pressure dependence of the output from charge transfer lasers but also suggest the general importance of three-body ion-molecule reactions in higher pressure plasmas.

CHAPTER II

THEORY

Preliminary Concepts

The key parameter throughout all discussions of reaction kinetics is the value of the reaction rate. The term "reaction rate" may be defined from the equation

$$\frac{dx}{dt} = k \cdot f(a,b,c...) \quad , \tag{2.1}$$

where k is termed the "rate coefficient" which could be a function of pressure or temperature, or perhaps other parameters and a, b, c... represent the concentrations of the reactants A, B, C... at time t. The function f(a,b,c...) represents some mathematical expression, usually a product of concentrations, that is a characteristic of the reaction. In the simple cases involving two reactants A and B, the explicit form of the function is f(a,b)=[A][B] where the brackets denote concentrations. Finally, the reaction coefficient is related to the collision cross section by the equation:

$$k = \int_0^\infty \sigma(v) \cdot v \cdot f\,(v) dv \quad , \tag{2.2}$$

where f(v) is the relative velocity distribution, $\sigma(v)$, the cross section for the collision, which will be discussed in the following section, and f(v)dv, the fraction of encounters in which the relative velocity v lies between v and v+dv. Therefore, if either k or $\sigma(v)$ is known the other can be found in most cases of practical interest.

As a typical example, let us consider the reactions between the two components

$$He_2^+ + X \rightarrow \text{Products} \quad , \tag{2.3}$$

together with the analogous three body reaction process

$$He_2^+ + X + He \rightarrow \text{Products} \quad , \tag{2.4}$$

where X is the secondary reacting species. The expressions for the rates of reaction are, respectively,

$$-\frac{d[He_2^+]}{dt} = k_2 [He_2^+][X] \quad , \tag{2.5}$$

and

$$-\frac{d[He_2^+]}{dt} = k_3 [He_2^+][He][X] \quad , \tag{2.6}$$

where k_2 is the binary rate coefficient defined in units of $cm^3 sec^{-1}$ and k_3 the ternary rate coefficient in units of $cm^6 sec^{-1}$. The latter of the order of 10^{-28} to 10^{-32} units for typical reactions, in contrast to the binary rate

coefficients which are usually of the order 10^{-8} to 10^{-12} units. In many cases experiments can be performed to determine the rate coefficient either directly or indirectly.

However, the situation presented thus far is complicated when the other mechanisms in a decaying afterglow are considered. For example, in the study of collision processes occurring at thermal energies, one of the mechanisms playing a dominant role in the decay of low pressure plasmas is diffusion. In a highly ionized gas, the ionization density being higher than 10^7 - 10^8 particles/cm^3, the diffusion equation describing the transport of particles as a result of concentration gradients is given by[21]

$$\frac{\partial n}{\partial t} = D_a \nabla^2 n \quad , \tag{2.7}$$

where D_a is ambipolar diffusion coefficient, which characterizes the diffusive motion of the two charge carriers. It is expressed by the relation

$$D_a = \frac{D^+M^- + M^+D^-}{D^+ + M^-} \quad , \tag{2.8}$$

where the M's are mobilities and the signs refer to positive ions and electrons. In a real afterglow plasma, diffusion contributes to the loss of ions in addition to the reactive

losses, although conditions can be chosen so that one or the other predominates. In the example of the reactions in the pure helium plasma, the rate equation for the He_2^+ ion can be expressed as

$$\frac{d[He_2^+]}{dt} = k_s[He^+][He]^2 - k_r[Y][He_2^+][e] + D_a\nabla^2[He_2^+] , \quad (2.9)$$

where k_s is the rate coefficient for the formation of He_2^+ by the reaction,

$$He^+ + 2He \rightarrow He_2^+ + He \quad , \quad (2.10)$$

k_r is the recombination rate coefficient of He_2^+ with electron by the reaction,

$$He_2^+ + e + Y \rightarrow He_2^* + Y \quad , \quad (2.11)$$

where the third body, Y, is needed to stabilize the capture of the electron, and the last term is the transport term. Theory[22] predicts that D_a varies inversely with the pressure if the electrons and ions are in thermal equilibrium with the gas at a temperature that is held constant as the gas pressure is varied. Thus at sufficiently high pressure, the transport term is negligible, and so is the source term because of the rapid conversion of He^+ into molecular ions, He_2^+, according to reaction (2.10). The equation (2.9) is then simplified to

$$-\frac{1}{[He_2^+]}\frac{d}{dt}[He_2^+] = k_r[e][Y] \quad , \tag{2.12a}$$

or to

$$-\frac{d}{dt}(\ell_n[He_2^+]) = k_r[e][Y] \equiv \nu(t) \quad , \tag{2.12b}$$

where $\nu(t)$ is defined to be the destruction frequency of the ions, or inverse lifetime of the ion concentration, due to recombination. To this basic equation describing the loss of He_2^+ ions in pure helium must be added terms such as those of eq. (2.5) and eq. (2.6) describing the reactive losses when other gas atoms of molecules are added to the afterglow. These modifications are discussed in the following sections.

Theory of Charge Transfer Process

Classical Langevin Theory

The charge transfer reaction can be studied theoretically within the framework of quantum mechanics, but it has been shown that its applications to specific processes may be possible only after the introduction of drastic approximation. A basic idea in the development of the theories of charge transfer reactions is that the electronic motion can be averaged over the time of collision because of the rapidity of the electronic motion in comparison to the nuclear

motion. As a result, the motion of the two nuclei can be treated classically.

In general, the charge transfer reactions which have been studied are the processes of symmetrical resonant charge transfer between atomic ions and atoms,

$$A^+ + A \rightarrow A + A^+ \quad , \tag{2.13}$$

and asymmetrical, nonresonant charge transfer reactions,

$$A^+ + B \rightarrow A + B^+ + \Delta E \quad , \tag{2.14}$$

where ΔE is the energy difference in ionization potentials between the initial and final states with the particles at infinite separation. The latter case of asymmetrical charge transfer was first considered by Giomousis and Stevenson[11] who developed a method of estimating ion-molecule reaction rates. They proposed a model for ion-molecule reactions which was an application of the kinetic theory of gases using the notion of the Langevin cross section[23] derived from a simple classical orbiting model.

Langevin's simplified orbiting model assumed that the ion is a point charge, since the electron does not deflect the moving ion to any significant extent, and that the ion-molecule potential function is dominated by the strong polarization forces,

$$V(r) = - \frac{\alpha e^2}{2r^4} \quad , \tag{2.15}$$

where r is the internuclear separation, e is the charge of the ion and α the electric polarizability of the molecule. Then the ions and spherical molecules moving under the given potential field were assumed to trace out classical trajectories determined by two parameters, the relative velocity, v, and the impact parameter, b. For these orbits there was found to be a critical value of b_o which led to a circular orbit of the ion around the molecule with radius $r = \frac{b_o}{\sqrt{2}}$. For $b \leq b_o$, the ion was found to spiral inwards until the repulsive forces between the electronic shells of the two particles repelled the colliding pair or until a chemical reaction occurred with subsequent separation of the products. This critical value of b_o was obtained by applying: (1) equilibrium conditions to the circular orbit, (2) angular momentum conservation and (3) energy conservation. The resulting expression

$$b_o = \left(\frac{4\alpha e^2}{mv^2}\right)^{1/4} , \qquad (2.16)$$

was derived with m being the reduced mass of the ion and molecule. Now if there exists a critical nuclear separation r_c which is less than $\frac{b_o}{\sqrt{2}}$, such a reaction must occur for separations within r_c, the cross section for the reaction is assumed to be the same as the cross section for orbiting collisions:

$$\sigma = \pi b_o^2 = \frac{\pi}{v} \left(\frac{4\alpha e^2}{m}\right)^{1/2} \quad . \tag{2.17}$$

The rate coefficient, with which the experiment is normally concerned, can then be obtained by using eq. (2.2), since the macroscopic rate coefficient is an average overall possible value of the relative velocity, v.

Giomousis and Stevenson[11] considered the process,

$$A^+ + BC \rightarrow AB^+ + C \quad , \tag{2.18}$$

and assumed that the space charge field produced by the electron beam was negligible so both velocity distributions were Maxwellian. The simple expression for the rate of production of secondary ion was obtained as,

$$\begin{aligned} \frac{dn_3}{dt} &= n_1 n_2 k \\ &= n_1 n_2 v\sigma(v) \\ &= 2\pi n_1 n_2 e \left(\frac{\alpha}{m}\right)^{1/2} \quad , \end{aligned} \tag{2.19}$$

where n_1, n_2 and n_3 were the number density of the primary ions, the molecules and the product ions, respectively. The rate coefficient k then was assumed to be the Langevin's value,

$$k = 2\pi e \left(\frac{\alpha}{m}\right)^{1/2} = 2.34 \times 10^{-9} \left(\frac{\alpha}{m}\right)^{1/2} \quad . \tag{2.20}$$

There are limitations on this classical description of ion-molecule reactions. First is that the polarization, r^{-4},

interaction may not be the leading term of v(r) but may, rather, depend on the type of molecule with which the ion is interacting. Of more concern in the development of above theory is the assumption that a chemical reaction always occurs on every collision within a region described by the critical radius r_c. The microscopic cross section for an ion-molecule reaction can be expressed better as

$$\sigma(v) = p\sigma_o(v) \quad , \tag{2.21}$$

where p is the probability that the reaction will occur if orbiting occurs. This probability, p, is assumed to be unity in the Langevin theory. Therefore, that model provides only upper limits for charge transfer rate coefficients and has generally failed to predict the absolute value of the rate coefficient.

Resonance Considerations

Charge transfer in ion-molecule reactions of highly exothermic systems has been known to be an efficient process for producing excited molecular ions. However, it is very often assumed that charge transfer in such systems can have a large cross section only if a resonance exists between the energy of the ground state of the primary ion and a particular vibrational and rotational level in an electronically excited state of the neutral molecule such that the energy defect is on the order of a few wavenumbers. This

assumption is mainly based on the approximate expression of the maximum cross section for calculating the thermal energy charge transfer reaction developed by Bohme, et al.[24,25] That expression, which incorporates the energy defect with the Langevin cross section, is given by

$$\sigma = \sigma_L(v) \exp K'(1 - \frac{A|\Delta E|}{hv}) \quad , \tag{2.22}$$

where σ_L is the value of the Langevin cross section for the ion-molecule reaction, K' and A are constants, h is Plank's constant, v is the relative velocity and ΔE is the energy defect at infinite separation for the case when the reactant and product molecules are in their ground vibrational and rotational state. However, because ΔE is actually a function of the separation of the colliding particles it is difficult to predict the most probable reaction simply by considering the energy defect at infinite molecular separation. For example, if energy defects, ΔE_{eff}, which are effective during the collision process, are assumed equal to those maintained at infinite nuclear separation, ΔE_{∞}, this may lead to serious errors for the simple reason that the inward spiralling orbits may modify the nuclear separations, r, over which the transitions take place. Therefore, the correct value of ΔE should correspond to that for the separations at which the transition most probably occurs. Unfortunately, the relevant energy defects at the specific

reaction distances are almost always unknown. Nevertheless, the requirement remains that a resonance must exist with a level of the molecular ion having a favorable Frank-Condon overlap with the neutral molecule.[26] Whether both of these requirements play important roles for a particular charge transfer reaction or either of these dominates over the other has not been fully investigated, to date.[26,27] Nevertheless, it seems clear that Frank-Condon factors must be important in high energy charge transfer reactions, while they may not be as important at thermal energies because of the higher possibilities for long interaction times.

Figure 1a shows a typical energy level diagram from which the resonances of the ions of helium with the upper state of the nitrogen ion laser transition, the $B^2\Sigma_u$ state of N_2^+, can be readily appreciated. Figure 1b, 2 and 3 show energy level diagrams for the long-lived active species of helium and the possible product states of CO, Ar, Ne, CO_2 and CH_4. In each figure, the most probable energy state available for transfer from primary energy storing species are indicated by arrows.

Extension to the Present Work

It is useful in applying the techniques inferred in the previous sections to first consider in greater detail the reaction processes affecting the He_2^+ population in a pure helium afterglow.

Helium Ion Formation

Since helium is a naturally monoatomic gas, ionizing events first produce atomic ions. The molecular ions are then formed either by termolecular association,

$$He^+ + 2He \rightarrow He_2^+ + He \quad , \tag{2.10}$$

or by recombination,

$$He^+ + e + X \rightarrow He^* + X \quad , \tag{2.23}$$

where X is a third body and the asterisk denotes an excited state, followed by associative ionization,

$$He^* + He \rightarrow He_2^+ + e \quad , \tag{2.24}$$

where He^* denotes an excited state with energy equal to or above that of the appearance potential He_2^+. A number of investigations[28,29] have indicated that the process (2.24) is a nearly resonant reaction, resulting in molecular ions in an excited vibrational state, v=4 for the $3\ ^1D$ level. However, associative ionization, (2.24), is generally negligible compared to the ion conversion reaction, (2.10), because of the very small concentrations of the excited atomic species. Therefore, reaction (2.10) would seem to be the primary process contributing significantly to the production of He_2^+ in the pressure range of this experiment. The frequency of conversion of He^+ into He_2^+ is given[30] by

βp^2, where p is the helium pressure. The temperature dependence reportedly[31] goes as T^{-1}, where T is the absolute temperature. It follows, thus, that the times required for these reactions (2.10) to go to completion are minimized at low gas temperatures and high pressures. However, these are just the conditions favoring further association of the ions according to the scheme,

$$He_n^+ + 2He \rightleftarrows He_{n+1}^+ + He \quad , \tag{2.25}$$

for $n \geq 2$. Reaction (2.25) must be considered reversible because of the very low binding energies of additional helium atoms. Though little is known about the larger helium ion clusters, He_n^+, both experiment[32] and theory[33] agree that such clusters are stable, at least for n=3 and 4.[34]

Helium Ion Clusters

Theory supported by observations of fluorescence[9,19] from products of charge transfer reaction for helium ion-molecule reactions indicate that in some cases the fluorescent transitions in product ion are pumped by the resonant transfer of energy from the diatomic helium ion, He_2^+. More recently, however, the importance of helium ion clusters and their subsequent involvement in the ion molecule reaction chain has been suggested by Collins, et al.[35]

Although relatively little energy is lost in successively binding additional helium atoms to the ion for n > 2, the energy available for transfer is reduced substantially because of the repulsive energy between pairs of neutral helium atoms[36] remaining at small internuclear separations after any transfer reaction. Thus, it can be expected that if given reaction is exothermic with respect to charge transfer from He_n^+ then resonance will be improved by the successive ionic association implied by (2.25) until the reaction finally becomes endothermic. In the example of the helium-nitrogen bimolecular charge transfer reactions,

$$He_n^+ + N_2 \rightarrow N_2^+(B^2\Sigma_u) + nHe \quad , \qquad (2.26)$$

the successive associations of reaction (2.25) tend to bring a closer resonance with the v=0 level of the B state of N_2^+ for He_3^+ than for He_2^+, but preclude the reaction for n=4 by making it endothermic. Other similar systems may offer the possibilities of even closer resonance.

Continuity Equations

Most of the available information on helium ion clusters has been obtained from drift tube experiments[32] conducted in relatively tenuous plasmas at temperatures below 200° K and at pressures of 10-20 torr. The rate coefficient for conversion of He_2^+ to He_3^+ has been estimated to be greater than that for conversion of He^+ to He_2^+. Those results indicated

that helium ion aggregates, notably He_3^+, tend to form as rapidly as a result of termolecular reactions of He_2^+ as He_2^+ forms from He^+. The equilibrium constant was measured in those experiments and as a consequence of the relatively low range of pressures examined, the He_3^+ concentration was found to be insignificant at other than cryogenic temperatures. However, if these low-pressure results are extrapolated to atmospheric pressures of helium, even at 300° K, as much as 10 percent of the helium ion concentration can be expected to be triatomic after very short times. This, then, suggests that since populations of the various helium ion clusters cannot be readily decoupled at the pressures characteristic of the experiments reported here, the possibility of the simultaneous occurrence of reaction (2.26) for n=2 and 3 must be considered.

The continuity equations for the time rate of change of ion populations resulting from (2.25) and (2.26) can be written for n=2 and 3 as

$$\frac{d[He_2^+]}{dt} = -\nu_2[He_2^+]-\beta p^2[He_2^+]+k_D[He_3^+]+D_a\nabla^2[He_2^+] \quad , \qquad (2.27a)$$

$$\frac{d[He_3^+]}{dt} = -\nu_3[He_3^+]+\beta p^2[He_2^+]-k_D[He_3^+]+D_a\nabla^2[He_3^+] \quad , \qquad (2.27b)$$

where ν_2 represents the destruction frequency of $[He_2^+]$,

$$\nu_2 = \nu_o + k[N_2] \quad , \qquad (2.28)$$

caused by reaction (2.26) for n=2. It is described by the rate coefficient k with the ν_o providing the flexibility of including the effects of other first order losses of He_2^+. Further, in (2.27a) and (2.27b) the forward reaction for (2.25) is described for n=2 by the rate coefficient βp^2, and ν_3 represents the destruction frequency of He_3^+ in a manner analogous to ν_2 for He_2^+. k_D is the rate coefficient for dissociation of He_3^+ by the reverse reaction for (2.25). In local thermodynamic equilibrium the reaction (2.25) would be represented by

$$[He_2^+]\beta p^2 = [He_3^+]k_D \quad . \tag{2.29}$$

Thus, it follows,

$$k_D = \frac{[He_2^+]}{[He_3^+]}\beta p^2 \quad , \tag{2.30}$$

or,

$$k_D = \frac{\beta p^2}{R} \quad , \tag{2.31}$$

where $R=[He_3^+]/[He_2^+]$ at equilibrium. Therefore, equation (2.27a) and (2.27b) take the forms,

$$\frac{d}{dt}[He_2^+] = -\nu_2[He_2^+] - \beta p^2[He_2^+] + \frac{\beta p^2}{R}[He_3^+] \quad , \tag{2.32}$$

$$\frac{d}{dt}[He_3^+] = -\nu_3[He_3^+] + \beta p^2[He_2^+] - \frac{\beta p^2}{R}[He_3^+] \quad , \tag{2.33}$$

where the transport terms have been neglected because of the high pressures. The solutions of this coupled set of rate equations for the decay of the "normal modes"[37] of the populations give, to a high degree of approximation, that the sum of the populations of the ions should decay as

$$[He_3^+] + [He_2^+] = C \exp\{-(\nu_2+R\nu_3)t/(1+R)\} \quad . \qquad (2.34)$$

The difference between the $[He_3^+]$ and its equilibrium value, $R[He_2^+]$, should decay as

$$R[He_2^+] - [He_3^+] \equiv A \exp\{-\beta p^2 t(1+R)/R\} \quad . \qquad (2.35)$$

The degree of approximation is of the order of $\nu R/\beta p^2$ which is significantly less than 1% at pressures over 200 torr. In the range of pressures of interest in this work $\beta p^2/R$ will be of the order of $10^9 sec^{-1}$ when β is estimated from the corresponding value[38] for the termolecular association of He^+. Thus, equation (2.35) implies that departures from the equilibrium ratio of He_3^+ to He_2^+ will be erased at a rate of $10^9 sec^{-1}$ and, provided other destruction frequencies of these populations are significantly smaller, equilibrium populations of the helium ion clusters for $n \geq 2$ must be expected.

Equation (2.34) implies that the total molecular ion population undergoing charge transfer reactions will decay in the absence of external sources at a rate given by the

weighted mean of the reaction rates of each individual species. Since the equilibrium population of He_2^+ should exceed 90% over the 300 to 1500 torr pressure range of interest in these experiments, barring the occurrence of a rate coefficient for the reaction of He_3^+ an order of magnitude in excess of the Langevin limit, the loss of either the total helium molecular ion concentration, or $[He_2^+]$, should be controlled by the reactions of He_2^+. The He_3^+ population can be expected to play the role of a minor additional degeneracy of the He_2^+ state and the pressure dependence implied in the term $R\nu_3$ appearing in (2.34) should be negligible. Consequently, it can be expected that measurements of the rates of loss of $[He_2^+]$ populations, parametrically as functions of reactant concentration, can indeed yield rate coefficients for the reaction of He_2^+, reasonably unaffected by equilibrium populations of larger helium ion clusters.

In the first approach[20] to the practical problem of measuring populations of He_2^+ ions at atmospheric pressure, the transient ion concentration was monitored by observing the time-resolved radiation from excited states of He_2, formed by the collisionally stabilized recombination of the He_2^+ with electrons. However, this technique is rather difficult in application, because of the complex relationship between the recombination radiation and the $[He_2^+]$,

and an alternate scheme is suggested by prior reports[7,8,9,19] of intense fluorescence emitted from product states formed as the result of charge transfer from He_2^+ in low pressure afterglows. In a reaction such as (2.26), if the destruction frequency, ν_d, of the product $N_2^+(B^2\Sigma_u)$ populations is greater than ν_2, the reaction frequency of the reactants, the population of products will first decay at the faster rate until the population approaches the quasi-equilibrium value

$$[N_2^+(B)] = (\nu_2/\nu_d)[He_2^+] \quad . \tag{2.36}$$

After that time the population of $N_2^+(B)$ will "follow" the evolution of the He_2^+ concentration and spontaneous radiation from that product state will serve as a convenient monitor of the ion concentration.

In practice the necessary condition $\nu_d >> \nu_2$ is not difficult to fulfill as the concentration of reactant admixture to the helium can be made arbitrarily small. Estimates of ν_d must include both the rate of spontaneous radiation and the rate of collisional quenching and studies of laser outputs pumped by (2.26) have indicated latter term dominates by nearly an order of magnitude. Since the lifetime for spontaneous emission is 66 nanosecond,[39] ν_d can be expected to be at least of the order of $10^8 sec^{-1}$ at atmospheric pressures in electron-beam plasmas. Thus, if the measured destruction frequency for the decay of the fluorescence from reaction

products is significantly smaller than $10^8 sec^{-1}$, it can be reasonably equated with the destruction frequency ν_2 of the He_2^+ concentration.

This then suggests the experimental procedure of adding a sufficiently small amount of nitrogen to a high pressure helium plasma and observing

$$\nu = \frac{1}{I} \frac{dI}{dt} \quad , \tag{2.37}$$

where I is the intensity of the transient fluorescence from the N_2^+ product states. Then provided $\nu << 10^8 sec^{-1}$, the identification can be made $\nu = \nu_2$. From (2.28) it follows that

$$k = \frac{\partial \nu}{\partial [N_2]} \quad . \tag{2.38}$$

Finally k must be examined for a possible dependence on helium pressure for it must be expected to have the form,

$$k = k_2 + k_3[He] \quad , \tag{2.39}$$

where k_2 is the rate coefficient for the binary reaction (1.7) and k_3 is the rate coefficient for the ternary reaction (1.9).

For the measurement of rate coefficient for the reaction of He_2^+ with species not yielding a convenient product fluorescence, a small fixed concentration nitrogen can be added as an indicator to monitor the He_2^+ concentration while the

concentration of the other species is varied. In that case the analog to (2.28) is written with the k rate coefficient for the desired reactant replacing that for N_2 and the constant contribution from the small concentration of the nitrogen is absorbed into the constant ν_o. Then if the partial differentiation of equation (2.32) is taken with respect to the varying concentration of desired reactant, the rate coefficient is obtained for the reactions of He_2^+ with that species. Resolution of the resulting coefficient still follows equation (2.33).

Although several possibilities beside nitrogen exist to monitor the He_2^+ ion concentration, the relatively large ν_d, large rate coefficient k, relatively small k_3, and high intensity of the resulting fluorescence proved decisive factors in the selection of this ion indicator. Generally 50 μ Hg nitrogen were added to the helium, and in the case of the subsequent addition of another reactant, its partial pressure was always kept low enough so that the total destruction frequency of equation (2.37) was less than $3 \times 10^7 sec^{-1}$ over the range of data needed to determine the rate coefficients. For most of the important data $\nu \leq 10^7 sec^{-1}$ and the models implied by equations (2.37), (2.38) and (2.39) were found to be completely consistent for ν up to $3 \times 10^7 sec^{-1}$ so that the identification of $\nu=\nu_2$ was considered confirmed.

CHAPTER III

EXPERIMENT

Apparatus

Figure 4 shows the high pressure cell with which these experiments were performed. It was constructed from stainless steel and had a 0.025 mm thick titanium window through which the electron beam entered. The 1/4" thick quartz windows were sealed by viton gaskets across the optical axis which was arranged to be perpendicular to the axis of propagation of the electron beam. A third window sealed across the end of the axis of beam propagation permitted the observation of the spectrum, integrated spatially along the axis of beam propagation. The cell was connected to a vacuum and gas handling system along the other axis perpendicular both to the direction of the beam propagation and to the optical axis.

A block diagram of the vacuum and gas handling system is shown in Figure 5. It included liquid nitrogen cooled traps which were filled either with glass wool for the removal of particulate contamination or with molecular sieves for gases purification. All components in the dashed line were Varian UHV-grade while the remaining parts were copper of

vacuum grade. Parts in the dotted line comprised a calibrated volume which provided for the accurate measurement of the pressures of the test gases. The thermistor gauge was used to check the ultimate pressure of the pumping system. As shown in the figure, the cold trap filled with molecular sieves was placed nearest to the pump. This trap functioned, primarily, to prohibit the transfer of pump oil vapor into the vacuum system and, secondarily, to pump, by condensation, water and other vapors which may have originated in the system. As a consequence, it was necessary to maintain a constant low temperature of the cryopumping surfaces in this trap to prevent pressure bursts resulting from the re-evaporation of condensate. The final system integrity was such that after baking with heating tapes the pressure rise in the sealed cell was less than 1 μ Hg over the time required for acquisition of a complete set of measurement made with a given gas sample.

The primary ionization of gases contained in the high pressure cell was produced by means of an electron beam, which propagated at 300 KV and entered the cell through the 0.025 mm thick titanium foil window. It was produced by a Field Emission Corporation model 706 electron gun which could emit 2×10^{14} electrons in a 3 nanoseconds pulse, nominally triangular in duration. Typically, a pulse was approximately 7 nanoseconds long with a half width of about

3 nanoseconds. The divergence of the beam was reported to be 30 degrees in angle.

The experiments performed with the system described above can be categorized in two parts. These are the time integrated spectral survey and the subsequent, time resolved intensity measurements for a particular component wavelength. In the first, spectra were recorded photographically with an f/6.3 Jarrell-Ash 0.75 meter Czerny-Turner spectrograph. This arrangement for obtaining time-integrated survey spectra is shown schematically in Figure 6. Five discharges were usually required for a useful exposure on Eastman 2485 film, developed to an ASA equivalent index of 8000. Slits were set to give 1 Å to 10 Å resolution, depending on the data taken.

In the second phase of data acquisition the transient intensity was measurements at a particular wavelength with an f/4 Jarrell-Ash 0.25 meter monochromator and a nine stage RCA-C31025C photomultiplier. The photomultiplier rise time of 1.5 nanoseconds insured that the transient intensity could be monitored with nanosecond resolution. As shown in Figure 7, the data acquisition and recording were handled by a Biomation model 8100 transient digitizer interfaced directly to an on-line Hewlett Packard model 2100 computer. The function of the model 8100 transient digitizer was to record successively defined time segments of an analog signal. It

provided the 8-bit digitation of input signals for a total recorded time of 2048 increments of the sample interval, at minimum 10 nanoseconds. As used in these experiments the overall time resolution was 10 nanoseconds and the resolution of intensity was one bit in 256, although in practice this was reduced to 1/128 of peak intensity by the practical inability to insure each data set reached full scale at maximum intensity. As shown in Figure 7, all data were acquired in an electrostatically screened room behind a lead shield to eliminate both RFI and X-ray noise. The total screening was adequate to reduce the noise recorded as a result of the electron-beam discharge to 2 percent of the detected optical signal for wavelengths of interest.

Procedures

Although the final verification of the integrity of the vacuum and gas handling system was obtained with a commercial helium leak detector, a more continuously operable check on the integrity of the system was necessary. This was done by periodically recording the spectrum of the electron-beam discharge into pure helium. This technique of photographing the spectrum will be discussed immediately after introduction of operating procedures.

The main procedural obstacle was to arrange an efficient way of operating the vacuum and gas handling system in order

to keep the system "clean", while filling with test gases and simultaneously measuring the pressures very accurately. Throughout the experiments, maintaining the high purity of sample gases was a stringent condition for obtaining significant and reproducible results. The initial purity of the helium was set by the choice of using the chromatograph grade supplied by AIRCO. This helium gas from a cylinder containing primarily 10 ppm of condensable impurities was further purified by passing it through a trap containing molecular sieves at liquid nitrogen temperature. Resulting purity was believed to be better than a few ppm. The purity of additive gases was equivalent to the Linde standard grade of 99.97 percent. They were further purified cryogenically to the extent consistent with their condensation temperatures.

In operation, the cell was always filled with minority gas first and high pressure helium next. In an example of operation, minority gas was first passed from the cylinder into the trap. From there it was passed through the inlet port, still being isolated from the cell. While the inlet port and manifold was filling, the pressure was monitored on the Wallace and Tiernan differential aneroid pressure gauge. The rate of filling with the gas was approximately 80 μ Hg per second. The small calibrated volume in the manifold was then sealed with the indicated pressure of the minority

gas being trapped in the volume. During all these steps, the cell was being continuously pumped through the liquid nitrogen cold trap. After the high pressure cell was isolated from the pump, it was filled from the calibrated volume through the valve. The pressure of minority gas was then determined from the calibrated ratio of expansion from the source pressure indicated by the Wallace and Tiernan pressure gauge into the total volume including the cell. This expansion ratio had been previously determined to be 0.0125, in terms of pressures.

In a second step the cell with a known pressure of minority gas was then isolated from the calibrated volume. The high pressure gas manifold was valved off from the pump and filled with helium to the desired pressure through a molecular sieve trap cooled to liquid nitrogen temperature. Then the high pressure cell was quickly filled through the valve and the valve was closed. While keeping the pressurized cell completely isolated, the rest of the system was then evacuated. After evacuation, the small calibrated volume was filled with the gas mixture from the cell and sealed. The total pressure of the gas mixture was then determined from the calibrated ratio of expansion from the calibrated volume to the evacuated volume containing the Wallace and Tiernan pressure gauge. This ratio of the calibrated volume to the total volume had been previously

determined to be $(32.2)^{-1}$. After data was taken, the measurement of the total pressure was repeated and served as a check on the leakage of the system under high pressure. Nevertheless, because of slight variance in valve closures coupled with gauge resolution and the relative high expansion ratio, errors as great as 5 μ Hg were expected occasionally.

The first diagnostic investigations conducted were spectral surveys to locate the wavelengths of the prominent features of the possible product states from charge transfer reactions. In the case of pure helium, these provided a very sensitive test for system purity, as mentioned early. For this part of the experiments a spectrometer with a low f-number was needed because of the inherent weakness of the fluorescent radiation from the transient plasma which radiated only for times comparable to the radiative lifetimes of the excited states of the reaction products. However, it was determined quickly that the 0.75 meter Jarrell-Ash spectrograph described in the previous section was capable of photographing spectra with sharp and well defined lines. That instrument had a nominal exit aperture of f/6.3 and an entrance aperture of f/4. As it is generally important that the light collection system be of the right combination of focal length and aperture, the focusing optics had to have an aperture of at least f/4 to fill the aperture of the spectrograph completely. Two concave mirrors, which had

apertures of f/4 were used instead of a lens in order to reduce loss due to absorption and reflection. All optical components were mounted kinematically on the optical bench attached to the spectrograph.

For the system arrangement to be in correct optical alignment, a He-Ne laser was first used to place the axis of the high pressure cell and the centers of focusing mirrors in co-planar alignment with the spectrograph. The entrance slit of the spectrograph, the two mirrors and high pressure cell were placed in the plane as closely as possible, so as to minimize the off-axis angle. A mercury source placed in the laser beam path was used for focusing purposes. To prevent scattered light and stray light from entering the optical system, the light shield was used as shown in Figure 6.

Figure 8 presents a survey spectrum taken of the afterglows of discharges into nominally pure helium at three different pressures. Principal features including impurities have been identified. Although trace impurities are seen, even further improvement in purity was achieved in the later stage of the experiments.

In the time-resolved emission measurements, techniques similar to those used for the spectral survey were used to obtain correct optical alignment. However, in this case

a quartz lens which had an aperture of f/4 was used for focusing the beam onto the entrance slit of the monochromator.

In operation during this part of experiment, it was determined that it was necessary to change the gas filling the cell after four successive discharges because of the onset of perceptible variation of the apparent lifetimes of the fluorescent intensities. Figure 9 shows an example of the time evolution of four successive pulsed excitations of the 4278 Å fluorescence in the electron-beam afterglow at 1 atmosphere of helium with 150 μ Hg of nitrogen. Displayed is the scope output of the transient recorder. Even though the photograph does not show the extreme cases, it was observed that the slope of the decaying profiles varied with an increasing number of discharges. In practice, data was used only from the first two discharges into a particular gas sample.

Systematic studies of the dependence of the measured logarithmic decay frequency, ν, on possibly spurious variables showed no effect on ν, as defined in Eq. (2.37) to result from linear attenuation of the optical beam, from changes of digitization range, or from changes of photomultiplier voltage, provided full scale deflection of the digitizer was avoided. Figure 10 presents typical lifetime profiles showing the decay of the logarithm of the intensity

of the spontaneous emission detected at 4278 Å as a function of time at a pressure of 818 torr helium containing 100 μ Hg nitrogen. The slopes of the lines determined by the data points shows the independence on spurious variables mentioned above.

Data obtained was reproducible to the extent consistent with the scatter seen in the following figures. Throughout the course of the experiment the ν for 50 μ pressure of nitrogen added to several different helium pressure was verified every second day. Only in the case of the last data set obtained, that for methane, was perceptible change noted in the base value of ν. This is seen in the data of the following chapter.

CHAPTER IV

EXPERIMENTAL RESULTS

Spectra

It has been mentioned in Chapter III that the spectrum of the afterglow of an intense electron beam discharge into pure helium showed both the atomic lines and molecular bands of helium resulting from the recombination of the helium ions with electrons. It was reasonable, then, to expect that the afterglow formed in high pressure helium samples containing traces of a second gas would be characterized by the additional development of parts of the spectrum of the second gas. Particularly, as a result of the charge transfer reactions,

$$He_2^+ + X \rightarrow \text{Products} \quad , \tag{4.1}$$

emissions from the product states of the minority constituents in near resonance with helium molecular ion, He_2^+, were expected with a high probability. However, these particular spectral systems were expected to occur either weakly or not at all when the same gas was excited in a pure state. The actual intensity of each spectral system expected as a result of the charge transfer reaction (4.1)

should, of course, depend on the pressure of the minority constituent. The addition of an insufficient quantity would yield a very low intensity because of competing channels for the destruction of the helium ions, while the addition of an excess of the reactant gas would also result in a low intensity because the primary discharge would directly excite the secondary gas without any selectivity.

In the example of He-N_2 mixture, provided the partial pressure of minority constituent was low enough to complete the reaction (2.10), the ionization was expected to convert from He^+ to He_2^+, thus making available the charge transfer reaction (4.1). Figure 11 shows the resulting spectrum for the cases of an electron-beam discharge into two samples of nitrogen, 1 torr and 50 torr, diluted in 1 atmosphere of helium. For the lower partial pressure of nitrogen, the strong selective excitation of the First Negative system of N_2^+ is seen, while the intensities of the selective excitations are reduced for the higher partial pressure. This is in agreement with the expectations discussed above. The transition which gives rise to this system is the $B^2\Sigma_u^+ \rightarrow X^2\Sigma_g^+$ electronic transitions of N_2^+. The component bands are blue-degraded and the three most prominent sequences occur in the wavelength region 3914 Å (0,0), 4278 Å (0,1) and 4709 Å (0,2), where the numbers in parentheses give the initial and final vibrational quantum numbers. As can be seen

in the figure, these were clearly the most dominant features observed in the case of the optimal partial pressure of nitrogen. However, even then, it was difficult to observe the First Negative system completely free from the Second Positive system of N_2^+. Since the Second Positive system of N_2^+ is very easily excited in almost any type of discharge through pure nitrogen or through a gas mixture containing a trace of nitrogen, the appearance of the system was attributed to the direct electron impact excitation of the ground state nitrogen molecules.

The spontaneous emission spectra from an electron beam discharge into two samples of carbon monoxide, 1 torr and 50 torr, diluted in 1 atmosphere of helium are shown in Figure 12. The emissions expected on the basis of energy level diagrams and resonance considerations were the First Negative system of CO^+, the $B^2\Sigma \rightarrow X^2\Sigma$ electronic transition, and the Baldet-Johnson system of CO^+, the $B^2\Sigma \rightarrow A^2\Pi$ transition. The most prominent sequences of the Baldet-Johnson system actually observed were the (0,0), (0,1) and (1,0) vibrational transitions. The First Negative system of CO^+ was not observed in the ultraviolet region. The features in the spectrum of a He-CO mixture, as seen in Figure 12, contained contributions from all nascent species resulting from free radical reactions occurring at later times in the afterglow.

Figure 13 shows the spectrum for the cases of electron beam discharges into two samples of carbon dioxide, 1 torr and 50 torr, mixed with one atmosphere of helium. The emissions expected were the $A^2\Pi_u \rightarrow X^2\Pi_g$ band system and the $B^2\Sigma_u^+ \rightarrow X^2\Pi_g$ band system of the CO_2^+ electronic transitions.[18] However, no emissions were detected from the $B^2\Sigma_u^+ \rightarrow X^2\Pi_g$ transitions of CO_2^+ which are known to consist of a single band, a doublet at 2882 Å and 2896 Å. Though a great deal of information on CO_2^+ is available in the literature, many of the bands reported have not actually been classified due to the complexity of the complete band system. The prominent features of the spectrum shown in the figure have been identified in terms of various progressions of the form $^2\Pi_u$ $(0,0,0) \rightarrow {}^2\Pi_g$ (n_1,n_2,n_3). The upper state is always $^2\Pi_u$ $(0,0,0)$ and, thus, only transitions to the different vibrational energy levels of the lower $^2\Pi_g$ state were involved.

Figure 14 shows the resulting spectrum of electron-beam excited gas mixtures of 1 torr and 50 torr of methane in 1 atmosphere of helium. As can be seen, in these cases the $(0,0)$ bands of the $A^2\Delta \rightarrow X^2\Pi$ electronic transition and the $(0,0)$ bands of the $B^2\Sigma \rightarrow X^2\Pi$ transition of CH appeared strongly in the spectra of the electron-beam discharges. No observations were made at other wavelengths.

The spectra from a discharge into the monoatomic inert gases in torr amounts in 1 atmosphere of helium showed the atomic lines. Figures 15 and 16 show the resulting spectra of electron-beam discharges into two samples of neon and argon, 1 torr and 50 torr, each, diluted in 1 atmosphere of helium. The strong 5852 Å line was particularly prominent in the case of neon, together with certain other portions of the spectrum of neutral atomic neon. No fluorescence spectra supporting charge transfer were observed from mixtures of helium with either of the monoatomic inert gas.

Table 1 summarizes the various major spectral systems observed in fluorescence in the visible wavelength region from the corresponding gases mixed in torr amounts into one atmosphere pressure of helium.

Time Resolved Spectral Intensities

It was found that a thorough examination of the fluorescence spectra from each of the gas mixtures was first necessary in order to avoid possible overlap of other afterglow fluorescence with the N_2^+ (B→X) transition used to monitor the time dependence of the ion concentrations. In fact, first attempts to acquire this data were complicated by such spurious effects leading to an apparent non-correlation of reactant and product channels in some cases.[40] Careful

TABLE I

SUMMARY OF THE SPECTRAL SYSTEMS OBSERVED IN THE VISIBLE WAVELENGTH REGION OF THE FLUORESCENCE FROM THE AFTERGLOW OF AN ELECTRON-BEAM DISCHARGE OF THE INDICATED GASES MIXED IN TORR AMOUNTS INTO ONE ATMOSPHERE OF HELIUM

Reactant	Spectral Systems	Charge Transfer	Source Comments
N_2	$N_2^+(B \rightarrow X)$	Yes	---
	$N_2(C \rightarrow B)$	No	Direct excitation of N_2
CO	$CO^+(B \rightarrow A)$	Yes	---
	C_2("SWAN")	No	Free radical chemistry
	C_2("high pressure")	No	"
CO_2	$CO_2^+(A^2\pi_u(0,0.0) \rightarrow X^2\pi_g(n.0,0))$	No	Unknown
CH_4	$CH(A \rightarrow X)$	No	Free radical chemistry
	$CH(B \rightarrow X)$	No	"
He	Ne(5852 Å)	No	Dissociative Recomb. of $HeNe^+$
	Ne*(Various)	No	"
Ar	Ar*(Various)	No	Unknown

attention to the spectral components emitted from each afterglow served to avoid this problem.

From the data of Table I it was concluded that none of those emissions could contribute spurious intensity at wavelengths closely corresponding to the band head at 4278 Å for the 0→1 vibrational component of the $N_2^+(B\rightarrow X)$ transition, even in triple component mixtures containing relatively little of the nitrogen to be used to monitor the He_2^+ concentration. In practice this was verified for the afterglow of each mixture of helium and other reactant by observing a digitized signal at 4278 Å less than 2 bits in the absence of nitrogen at any time of importance in the afterglow.

However, a reasonably narrow spectral resolution of 4-10 Å was required near 4278 Å to be certain to avoid spurious fluorescent components from the nitrogen itself. Figure 17 shows the variation as a function of wavelength of the destruction frequency, ν, defined by Eq. (2.37) in Chapter II, measured in a mixture of helium and nitrogen. Shown by the scale to the right of the figure is the corresponding peak intensity observed. The destruction frequency can be seen to be constant to within experimental scatter near the peak of intensity at the band head in the P-branch at 4278 Å. Conversely, some variation begins to show with decreasing wavelength from the second peak in intensity. Throughout the remainder of this experiment the wavelength used to monitor the He_2^+ concentration was chosen to be 4278 Å and the

spectrometer resolution of 4 to 6 Å was sufficient to reject spurious contributions to the experimentally measured destruction frequency. Measurements of the transient dependence of the intensity at 4278 Å were then taken as functions of helium pressure over the range from 300 to 1500 torr and as functions of the partial pressure of reactant from 25 to 500 μ Hg.

Typical Data for Binary Gas Mixtures

Figures 18 and 19 show typical data for the transient dependence of the intensity emitted spontaneously at 4278 Å from the afterglow of a mixture of helium and nitrogen. Displayed is a linear plot of the digital output from the Biomation 8100 transient digitizer used to store the record of transient fluorescence from a single electron-beam discharge into the gas. The scale of these data is 100 nanoseconds per horizontal division. Figures (18a) and (18b) were taken from afterglows in which the helium pressures were held constant and the nitrogen pressure were varied as shown. Results similar to these were recorded for the cases of the constant pressure of nitrogen with the different helium pressure, as shown in Figures (19a) and (19b). The resulting transients not only varied as functions of the partial pressure, but also differed as functions of the helium pressure. The significant variations were found

in a logarithmic plot of the digitized signals as shown in Figures 20, 21 and 22. Figures 20 and 21 show typical data for the transient dependence of the intensity at 4278 Å from the afterglow of 50 μ Hg and 200 μ Hg partial pressures of nitrogen diluted into the different pressures of helium, respectively. Figure 22 shows typical data for the transient dependence of the intensity emitted spontaneously at 4278 Å from the afterglow of 830 torr of helium containing the various partial pressures of nitrogen shown. Intensities have been normalized in these figures to avoid possibly confusing intersections. On this time scale the 3 nanoseconds duration of the electron beam discharge cannot be resolved. The pronounced curvature appearing at later times is believed to result from contributions from the Penning ionization of N_2 by the relatively smaller population of metastable $2\ ^3S$ helium atoms of lower reactivity. Values of destruction frequency obtained from later portions of the data than those shown in Figure 22 agreed roughly with values to be expected from known rate coefficients for Penning ionization. These data from the later portions of the intensity curves were not used in the work reported here.

From the slopes of the curves plotted in Figure 22 the corresponding values of ν were directly obtained as indicated by equation (2.37) in Chapter II. The consistency of the various values of destruction frequency could be readily examined by plotting the measured values of ν as functions of the partial pressure of the nitrogen reactant, as shown in Figure 23. This is a standard procedure in the study of chemical kinetics and from such a Stern-Volmer plot the appropriate value of reaction rate coefficient for charge transfer can be obtained. Provided the points representing the destruction frequency do not deviate critically from the line determining the rate coefficient, the intercept of this line gives the normal destruction frequency of the He_2^+ population in pure helium.

In the case of the data of Figure 23 obtained for 830 torr of helium, the reaction rate coefficient was found to be $1.4 \times 10^{-9} cm^3/sec$. It was, a priori, suggestive that this did represent the rate coefficient for the bimolecular charge transfer reaction in agreement with the ESSA value of $1.3 \times 10^{-9} cm^3/sec$. However, an examination of Stern-Volmer plots of data obtained from different pressures of helium did not support this concludion, but rather suggested the necessity of conducting a systematic study of the dependence of the rate coefficient on helium pressure.

It was considered that the acquisition from Stern-Volmer plots of a set of rate coefficients that was statistically dense with respect to variations of helium pressure would be prohibitively time consuming and an alternative procedure was adopted. In order to avoid any restrictive assumptions about the form of the dependence of destruction frequency on helium pressure, it was assumed that the dependence upon reactant concentration would be sufficiently linear that plots of ν as functions of helium pressure and only parametrically as functions of reactant concentration would be adequate for analysis. Figure 24 shows the resulting plot of data obtained for the destruction frequency as a function of helium pressure for two values of nitrogen concentration, 50 μ and 200 μ Hg. The apparent linearity of this data seemed to confirm its utility in the determination of charge transfer rate coefficients for the reactions described individually in Chapter V.

Typical Data from Ternary Gas Mixture

For gases other than nitrogen the changes due to the added reactant in the destruction frequency of the transient intensity of the 4278 $\mathring{A}$ radiation emitted from the "constant" 50 μ Hg component of nitrogen monitoring the He_2^+ concentration were used to obtain the desired reaction rate coefficients. In the case of methane the addition of various

partial pressures caused a clearly monotonic decrease in the lifetime of the He_2^+ population, as seen in Figure 25. In this figure intensities have not been normalized and the continuous decrease in the fraction of ions reacting to give nitrogen fluorescence is evident as the concentration of methane is increased. The data set denoted as having 0 μ Hg of methane corresponds to that for helium with only the 50 μ Hg of nitrogen. Values of destruction frequency were obtained from the data shown in Figure 25. Figure 26 presents the Stern-Volmer plot for methane which is analogous to that shown in Figure 23 for nitrogen. The intercept of the line determining the rate coefficient, for this case, gave the destruction frequency of He_2^+ population in a mixture of helium and nitrogen at 50 μ Hg. The rate coefficient for the destruction of He_2^+ determined by the slope of the linear fit to the data points was found to be $5 \times 10^{-10} cm^3/sec$ in good agreement with that reported in the literature.[20]

CHAPTER V

ANALYSIS AND CONCLUSIONS

Analysis

$He_2^+ + N_2$

Figure 24 in Chapter IV has shown the observed variation of the destruction frequency, ν, with helium pressure and parametrically with nitrogen concentration. The data shown represents the most comprehensive set obtained in the course of these experiments. Plotted are data obtained by taking the logarithmic derivatives of the transient intensities emitted in the $(0 \rightarrow 1)$ 4278 Å transition component, as well as in the $(0 \rightarrow 0)$ 3914 Å component of the $B \rightarrow X$ transition. Resulting values of ν are plotted as 0 and +, respectively. Data for both transitions from the same upper N_2^+ $(B^2\Sigma_u)$ state agree with the same linear approximations shown in Fig. 24, thus eliminating concern for any possible contribution to the intensity which might have resulted from stimulated emission, not linearly related to the upper state population. A few Stern-Volmer plots made at scattered values of helium pressure confirmed that the data lay in the range of linearity of the dependence on nitrogen pressure. Extrapolations of the data of Fig. 24

to zero nitrogen pressure implied a destruction frequency of He_2^+ in pure helium consistent with reasonable recombination rates plus a small dependence on helium pressure, most probably resulting from charge transfer to non-condensable impurities present in the helium at concentrations of a few microns per atmosphere, i.e., a few ppm.

The lack of parallelism in the data of Fig. 24 is most strongly indicative of the presence of a component in the destruction frequency proportional to both helium pressure and nitrogen partial pressure. From eq. (2.39) it can be seen that such a term is completely consistent with the representation, $k_3[He][N_2]$. Rewriting the ν_2 from eq. (2.27a) in terms of eq. (2.39) gives

$$\nu_2([He],[N_2]) = \nu_o + k_2[N_2] + k_3[He][N_2] \qquad (5.1)$$

so that in practice the bimolecular k_2 can be determined in units of cm^3/sec to be

$$k_2 = \frac{760}{0.15M_o}[\nu(0,200)-\nu(0,50)] \quad , \qquad (5.2)$$

where M_o is the Loschmidt number at room temperature. Then the termolecular rate coefficient can be written in units of cm^6/sec as,

$$k_3=(0.15P)^{-1}\left(\frac{760}{M_o}\right)^2\{[\nu(P,200)-\nu(P,50)]-[\nu(0,200)-\nu(0,50)]\} \qquad (5.3)$$

where P is the helium pressure in torr. Obtaining the values of ν appearing in eqs. (5.2) and (5.3) from the linear approximation to the data of Fig. 24 gave k_2 = 10.6 x $10^{-10}cm^3/sec$ and k_3 = 16±3 x $10^{-30}cm^6/sec$. It was found that $10^{-10}cm^3/sec$ and $10^{-30}cm^6/sec$ represented convenient scales for the bimolecular and termolecular rate coefficients, respectively, measured in this work and values obtained are presented in these units in the following material.

The data obtained for 50 μ Hg of nitrogen can be seen to exhibit the least scatter from the linear approximations shown in Fig. 24 and to display the greatest reproducibility. The corresponding linear approximation to that 50 μ Hg data was then considered to be an empirical base line describing the component of ν contributed by the constant, 50 μ Hg, concentration of nitrogen used to monitor the He_2^+ population through the relationship given by eq. (2.36). The departure from this base line caused by the reaction of He_2^+ with any additional gas added, either nitrogen or a third component, provided the changes in destruction frequency from which the rate coefficients were derived. Comparisons with previous measurements of rate coefficients were placed in perspective by considering the destruction frequency ν_e, defined by

$$\nu_e(P) = \nu(P,50) + \Delta p(760/M_o)^{-1}k_e(P) \quad , \qquad (5.4)$$

where $k_e(P)$ is the value of rate coefficient from the literature, originally measured at a helium pressure of P, and Δp is the partial pressure of reactant added to the mixture of helium and constant 50 μ Hg component of nitrogen indicator. Essentially, this comparative value consisted of the base value of destruction frequency of He_2^+ specific to this experimental apparatus, helium pressure and indicator plus an increase in destruction frequency computed from the product fo the comparative value of rate coefficient and the concentration of added reactant. In this case of $He_2^+ + N_2$ there were two values of k_e from the literature. The concentration of added reactant must be interpreted to be the 150 μ Hg of nitrogen added above the base value of 50 μ Hg. The resulting comparative values of ν_e are plotted in Fig. 24 at the appropriate helium pressure. It can be seen that the extrapolation of the data of this experiment is in complete agreement with the more recent of the two previous values to within the experimental uncertainty reported for that value. In fact it can be seen that the locus of intercepts at zero helium pressure of the possible linear approximations to the 200 μ Hg data is substantially smaller than the experimental uncertainty in previous measurements and the most probable uncertainty in the bimolecular reaction rate determined from this data is ±10%.

$He_2^+ + CH_4$

Figure 27 collects the results fo the measurements of ν as a function of helium pressure for CH_4 pressures of 50 and 200 μ Hg. In this figure the base line data corresponding to a zero methane component is plotted by the filled circles fitted by the linear approximation marked with the corresponding zero partial pressure of CH_4. This was the last reactant studied in this series and it showed the only variation in the base line observed. The value from Fig. 26 is shown by the dashed line for comparison.

Since two partial pressures of the admixture were obtained in addition to the base line, the data formed an overdetermined set for the extraction of the rate coefficients. This reduced the degree of arbitrariness in the linear approximations by requiring for consistency that

$$\nu(P,200) - \nu(P,0) = 4[\nu(P,50) - \nu(P,0)] \quad , \qquad (5.5)$$

where the second index here referred to the CH_4 partial pressure. The linear approximations shown in Fig. 27 are the best which were consistent with data sets at both pressures and eq. (5.5). The corresponding rate coefficients for

$$He_2^+ + CH_4 \rightarrow \text{Products} \quad , \qquad (5.6a)$$

$$He_2^+ + CH_4 + He \rightarrow \text{Products} \qquad (5.6b)$$

are $k_2 = 5.0 \times 10^{-10} cm^3/sec$ and $k_3 = 5 \pm 2 \times 10^{-30} cm^6/sec$, respectively. Accuracy of the bimolecular coefficient is apparently 25 percent.

$He_2^+ + Ne$ and $He_2^+ + Ar$

The reactions of He_2^+ with the monoatomic inert gases[13] were expected to be small and, hence present greater difficulty. Changes in destruction frequency caused by the added reactant were expected to be partially masked by random variation in the base ν_o.

Figures 28 and 29 show the resulting plots of destruction frequency as functions of helium pressure for 0, 50 and 200 μ Hg of added neon and argon, respectively. In these figures the base line is shown by the dashed line taken from the data of Fig. 24 and confirmed by the subsequent remeasurements plotted as filled circles. Linear approximations were constructed to be consistent with data sets at both partial pressures of reactant and eq. (5.5). Comparative values of ν_e have been derived from values of the bimolecular rate reported in the literature and are plotted together with the reported uncertainty at the appropriate pressure. It can be seen in the figures that the linear approximations to the 200 μ Hg data are completely consistent with the previous ESSA values.[13]

The case of neon is interesting because of the large variation in previous measurements of the bimolecular rate. Only the ESSA group[13] has reported a value larger than the traditional[6,20] $1.5 \times 10^{-10} cm^3/sec$. They attribute the smaller rate to the analogous reaction of neon with $HeNe^+$ formed later in the afterglow. Although the data of Fig. 28 indicates a larger rate, consistent with the ESSA value,[13] a more accurate measurement was attempted. The evident parallelism of the linear approximations argues for a small termolecular rate coefficient and suggests that a Stern-Volmer plot at any helium pressure in the pressure range of these measurements would be dominated by the bimolecular component. Figure 30 presents such a plot of data obtained at one atmosphere pressure and the straight line shown is consistent with a rate coefficient of $5.5 \times 10^{-10} cm^3/sec$. It is interesting to observe that at higher partial pressures of neon the destruction frequencies saturate and increase further at a rate more nearly consistent with the smaller value of rate coefficient. This was the only example observed to show a saturation and it is possible that this results from a conversion of the dominant ion from He_2^+ to $HeNe^+$. The resulting rate coefficients for the bimolecular and termolecular reactions of He_2^+ with neon were concluded to be $5.2 \times 10^{-10} cm^3/sec$ and $2\pm2 \times 10^{-30} cm^6/sec$, respectively.

In the case of argon the linear approximations of Fig. 29 gave rate coefficients for

$$He_2^+ + Ar \rightarrow \text{Products} \quad , \tag{5.7a}$$

$$He_2^+ + Ar + He \rightarrow \text{Products} \quad , \tag{5.7b}$$

of $k_2 = 2.2 \times 10^{-10} cm^3/sec$ and $k_3 = 24 \pm 6 \times 10^{-30} cm^6/sec$, respectively, making the termolecular reaction much more probable than the bimolecular. For both argon and neon experimental uncertainty in the bimolecular coefficients was estimated to be ± 30%.

$He_2^+ + CO$ and $He_2^+ + CO_2$

The reactions of He_2^+ with both CO and CO_2 presented the greatest technical difficulties. For reasons most probably associated with a tendency of the gases to be absorbed on surfaces and with the difficulty in degassing the various traps after each gas sample was prepared, reproducibility was poor. This is reflected in the data of Figs. 31 and 32. In the former the behavior of the destruction frequency at pressures above one atmosphere was completely anomalous, as can be seen by the open circles. Some improvement was obtained, however, by observing the evolution of the fluorescence of the B → A transition of CO^+ in binary mixtures of helium and CO. However, a rather complicated procedure was required to adapt the ν_c obtained from the weak CO^+

fluorescence from binary mixtures to the data of Fig. 31 obtained with the nitrogen indicator. Plotted as open triangles is an equivalent destruction frequency for a three gas mixture, ν_{eg}, obtained as follows:

$$\nu_{eg}(P,p) = \text{baseline} + \frac{p}{50}[\nu_c(P,100)-\nu_c(P,50)] \quad , \qquad (5.8)$$

where p is the CO pressure in torr, and, as mentioned above, ν_c was derived from measurements of CO^+ fluorescence in binary mixtures of helium and CO. As can be seen in the figure, the agreement between these equivalent data, ν_{eg}, and the open circles is good at the lower pressures and serves to assist in the derivation of a set of linear approximations consistent with eq. (5.5). Further the agreement indicates that the production of the B state of CO^+ is one of the possible output channels of the reactions

$$He_2^+ + CO \rightarrow \text{Products} \quad , \qquad (5.9a)$$

$$He_2^+ + CO + He \rightarrow \text{Products} \quad . \qquad (5.9b)$$

Rate coefficients of $10.8 \times 10^{-10} cm^3/sec$ and $36\pm8 \times 10^{-30} cm^6/sec$, respectively, were determined to be most consistent with the data.

The same pattern of large bimolecular and termolecular rate coefficients was displayed by CO_2. From Fig. 32 rates of $15.6 \times 10^{-10} cm^3/sec$ and $67\pm12 \times 10^{-30} cm^6/sec$ were found for these analogs of (5.9a) and (5.9b). For the bimolecular

reactions of He_2^+ with both CO and CO_2 accuracy was estimated to be ± 30%, and in both cases good agreement with the ESSA values can be seen.

Conclusions

The results of this work were found to be in good agreement with the values previously measured by the ESSA group at 200°K and, as shown in the figures of the preceding section, both values are well within the common region of overlapping uncertainties.

More important, however, is the identification and measurement of rate coefficients for the termolecular charge transfer reactions of the form,

$$He_2^+ + He + X \rightarrow \text{Products} \quad . \tag{5.10}$$

When rapid, these termolecular reactions offer significant parallel kinetic paths for the destruction of the He_2^+ ions in a helium plasma. Thus, the destruction frequency expected in a given plasma must be expected to contain contributions from both bimolecular and termolecular reactions and as a result, primary reaction paths for molecular helium ions can differ widely in high and low pressure plasmas and afterglows.

CHAPTER VI

SUMMARY

Values measured in this work for the bimolecular rate coefficients for charge transfer from He_2^+ are summarized in Table II together with previously reported values. Results obtained for the corresponding three body rate coefficients are summarized in Table III.

It appears particularly interesting that the presence of a third body can change an improbable charge transfer reaction involving He_2^+ into a very probable one, as in the case of the reaction with argon. For example, from Tables II and III it can be seen that less than a 300 torr pressure of helium is required to double the effective rate of reaction of argon with He_2^+ while over 3000 torr is required for CH_4.

It can also be expected that branching ratios among the possible reaction products will differ between the bimolecular and termolecular channels for the reactions of He_2^+ with a particular reactant. This seems to be the case in the reactions of nitrogen, with the termolecular reaction favoring a larger branching ratio into the $B^2\Sigma_u$ state of N_2^+. Thus, it appears that these larger termolecular charge transfer rates not only can serve to explain specific

TABLE II

SUMMARY OF BIMOLECULAR CHARGE TRANSFER RATE COEFFICIENTS FOR REACTIONS OF He_2^+ MEASURED IN THIS WORK TOGETHER WITH COMPARATIVE VALUES FROM THE LITERATURE.
UNITS ARE $10^{-10} cm^3/sec$.

Reactant	This Work	ESSA[13]	BLC[20]	Villarejo[41]	Oskam[6]
N_2	11	13	6	2.2	
CO	11	14	5.3		
CO_2	16	18	13		
CH_4	5		5.5		
Ar	2.2	2.0	2.5		
Ne	5	6	1.5	1.2	1.5

anomalous efficiencies of the charge transfer process observed in atmospheric pressure lasers but also suggests the general importance of three body ion-molecule reactions in higher pressure plasmas.

TABLE III

SUMMARY OF TERMOLECULAR CHARGE TRANSFER RATE COEFFICIENTS FOR REACTIONS OF He_2^+ MEASURED IN THIS WORK WITH THE REACTANTS LISTED. UNITS ARE $10^{-30} cm^6/sec$.

Reactant	Rate Coefficient
N_2	16 ± 3
CO	36 ± 8
CO_2	67 ± 12
CH_4	5 ± 2
Ar	24 ± 6
Ne	2 ± 2

APPENDIX

FIGURES

The figures described in this dissertation are given below.

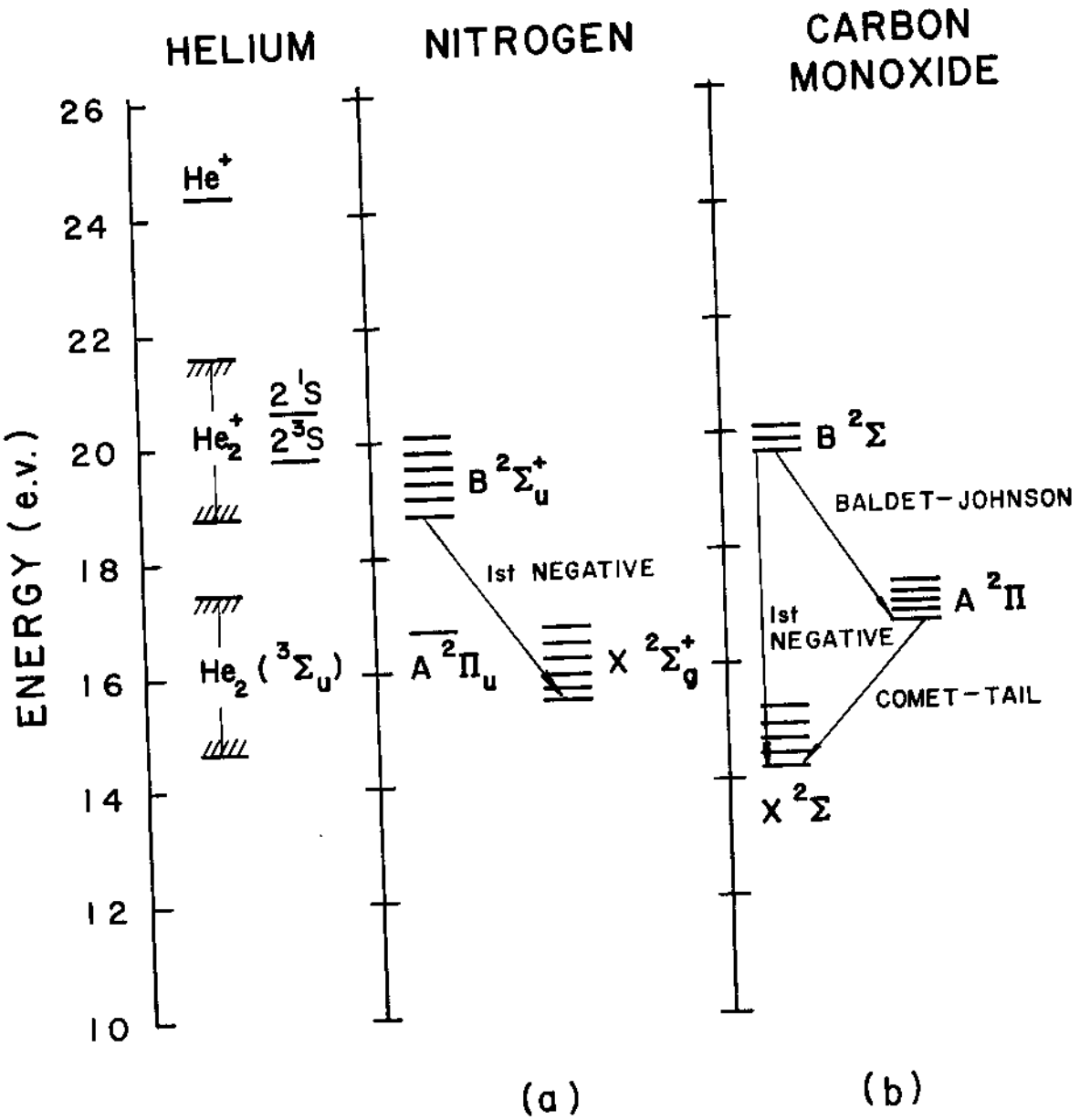

Fig. 1--Energy level diagram of the primary energy storing species of helium in comparison with the ion levels of nitrogen and carbon monoxide.

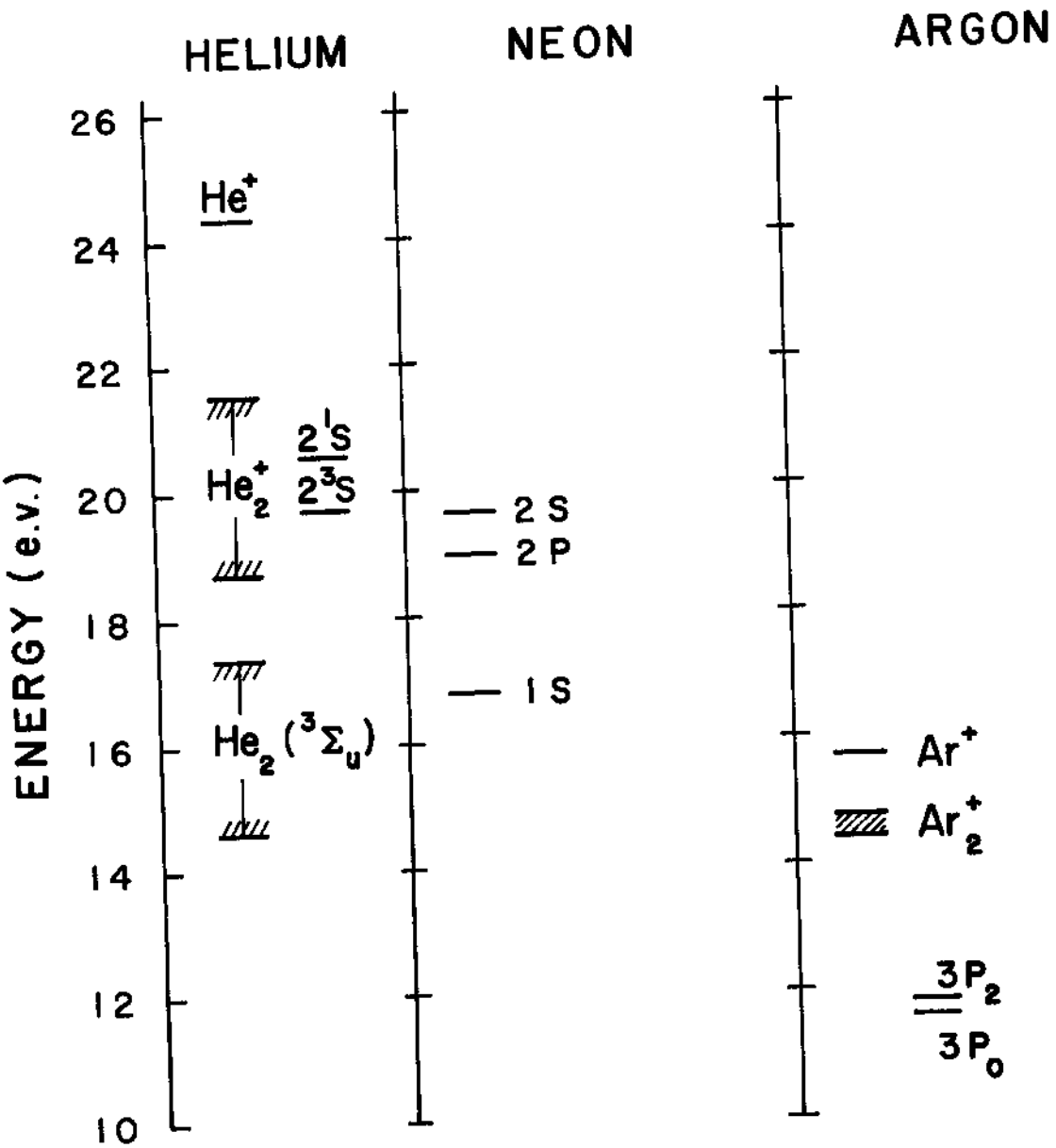

Fig. 2--Energy level diagram of the primary energy storing species of helium in comparison with pertinent energy levels of neon and argon.

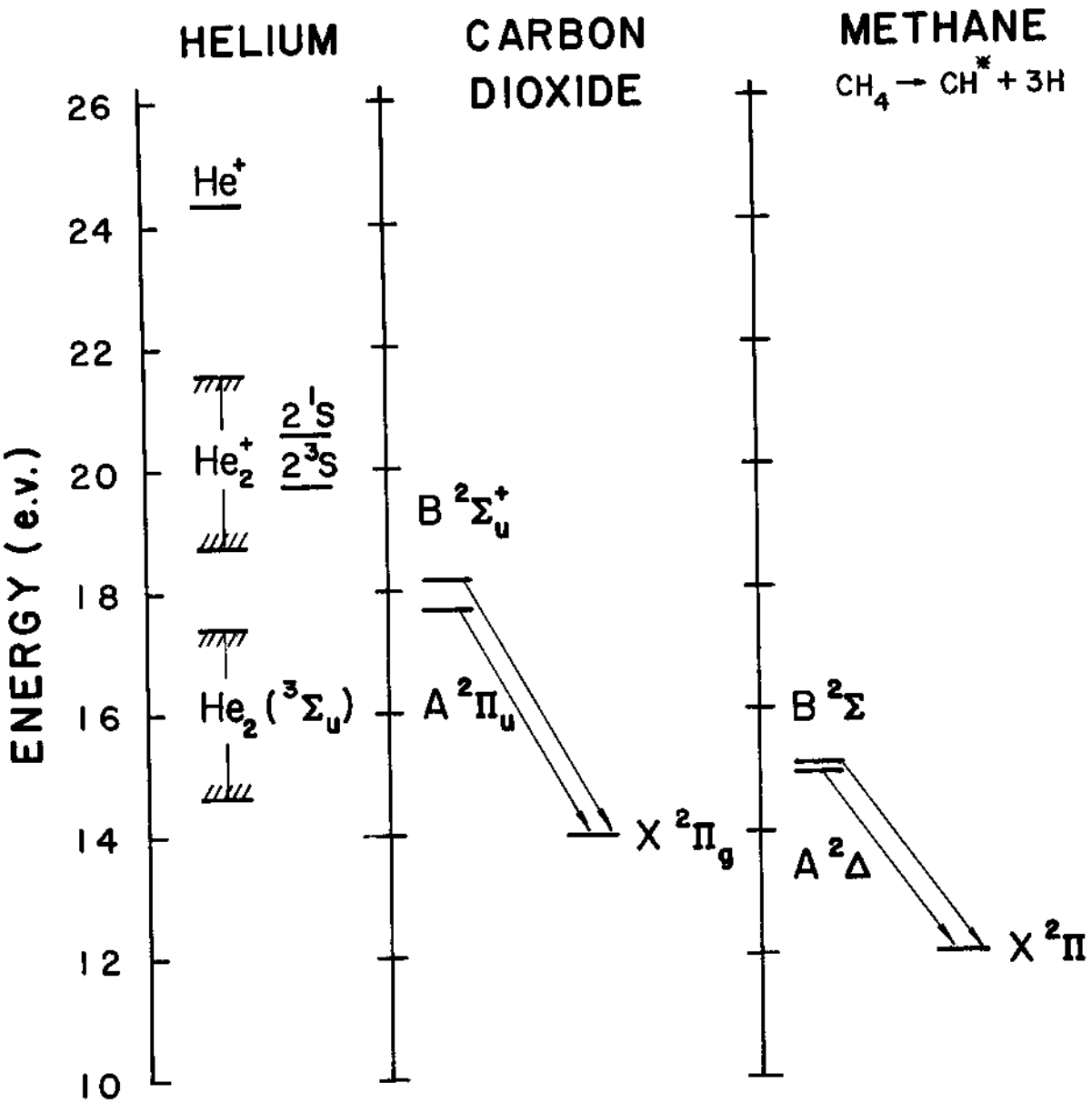

Fig. 3--Energy level diagram of the primary energy storing species of helium in comparison with pertinent energy levels of carbon dioxide and methane.

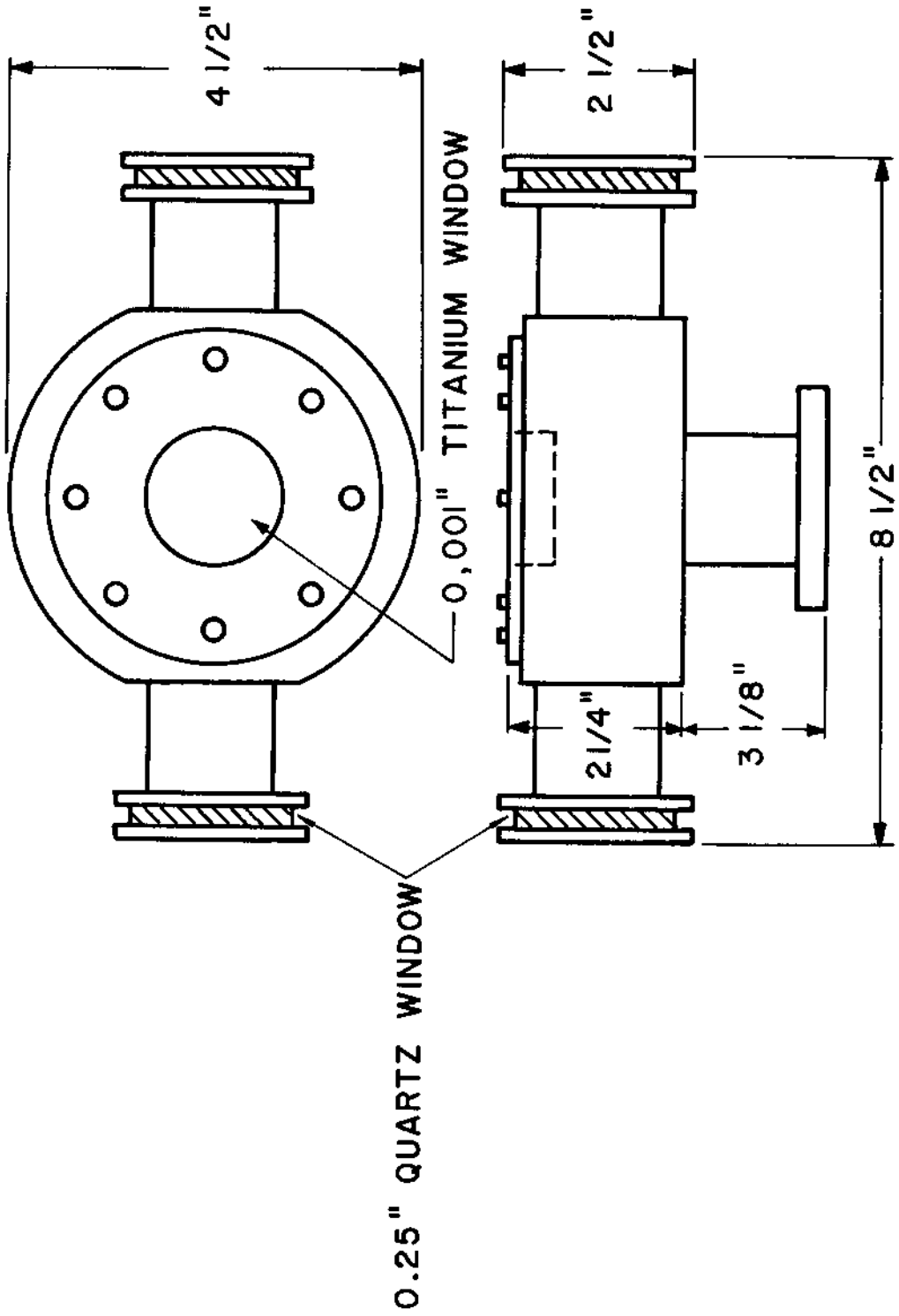

Fig. 4--High pressure cell

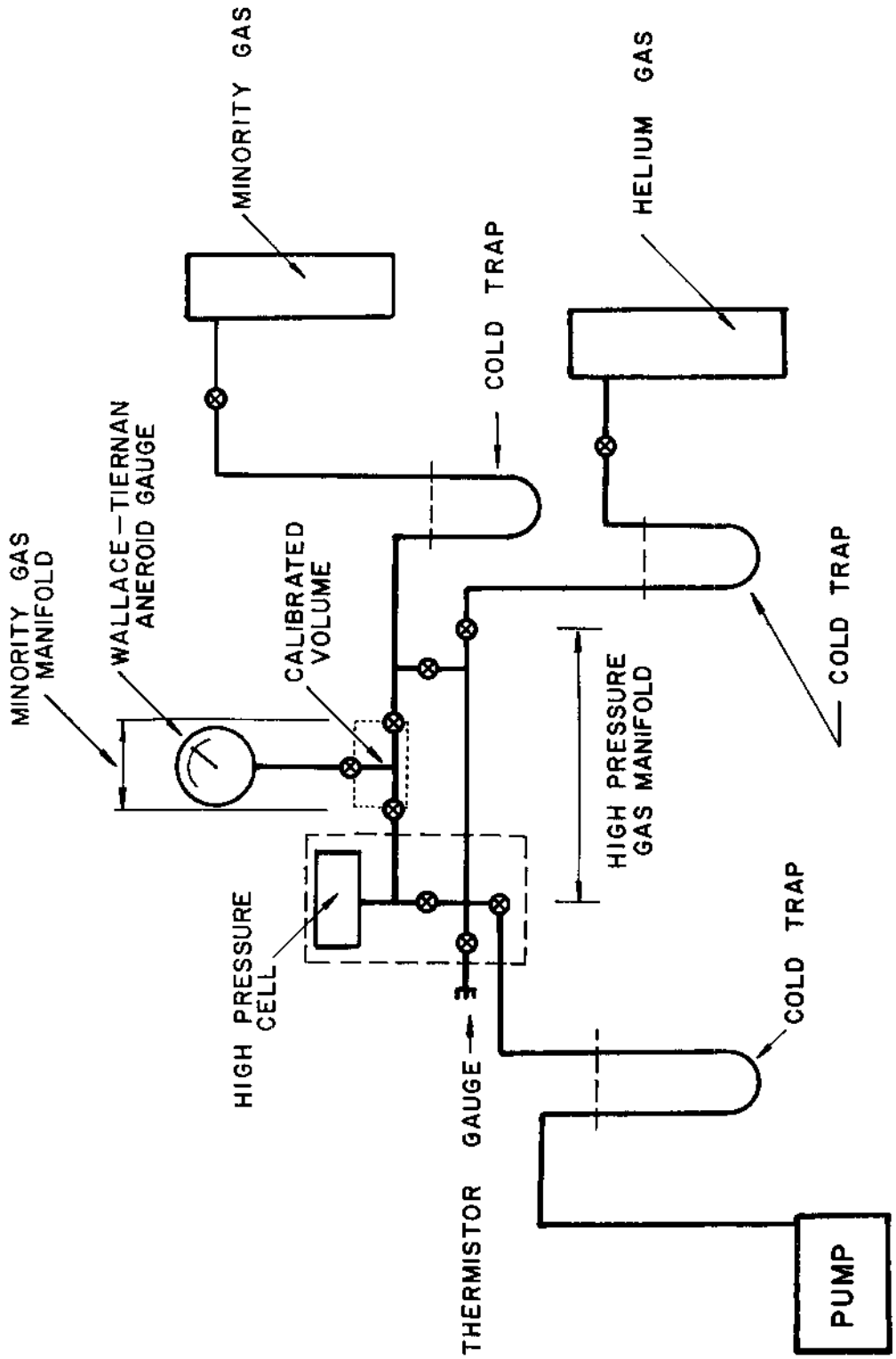

Fig. 5--Schematic diagram of the vacuum and associated gas handling systems

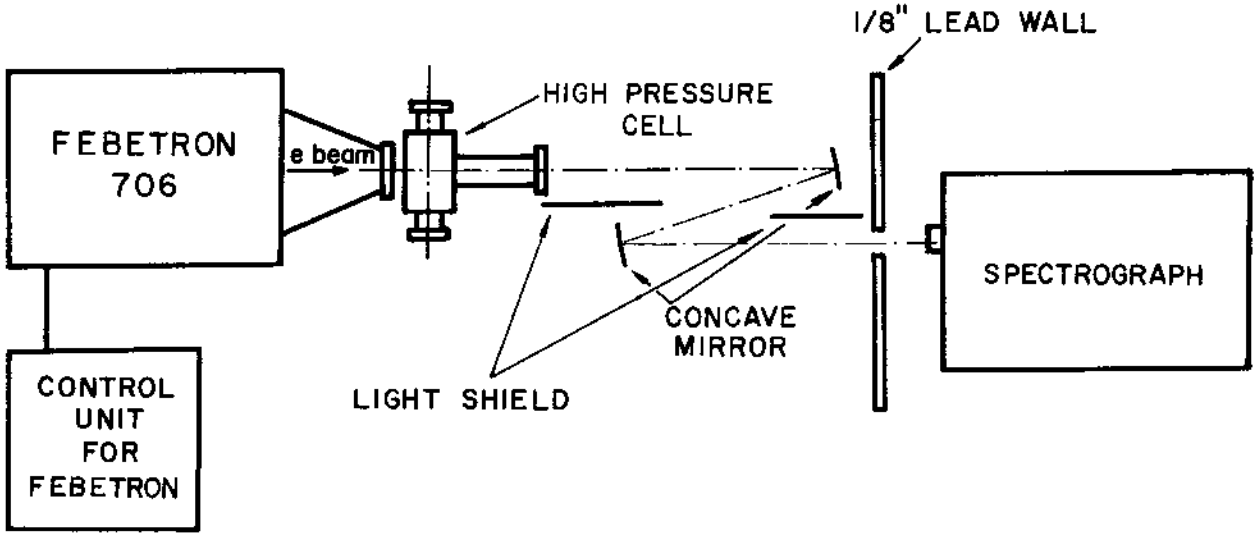

Fig. 6--Schematic diagram of the arrangement for time integrated survey spectra.

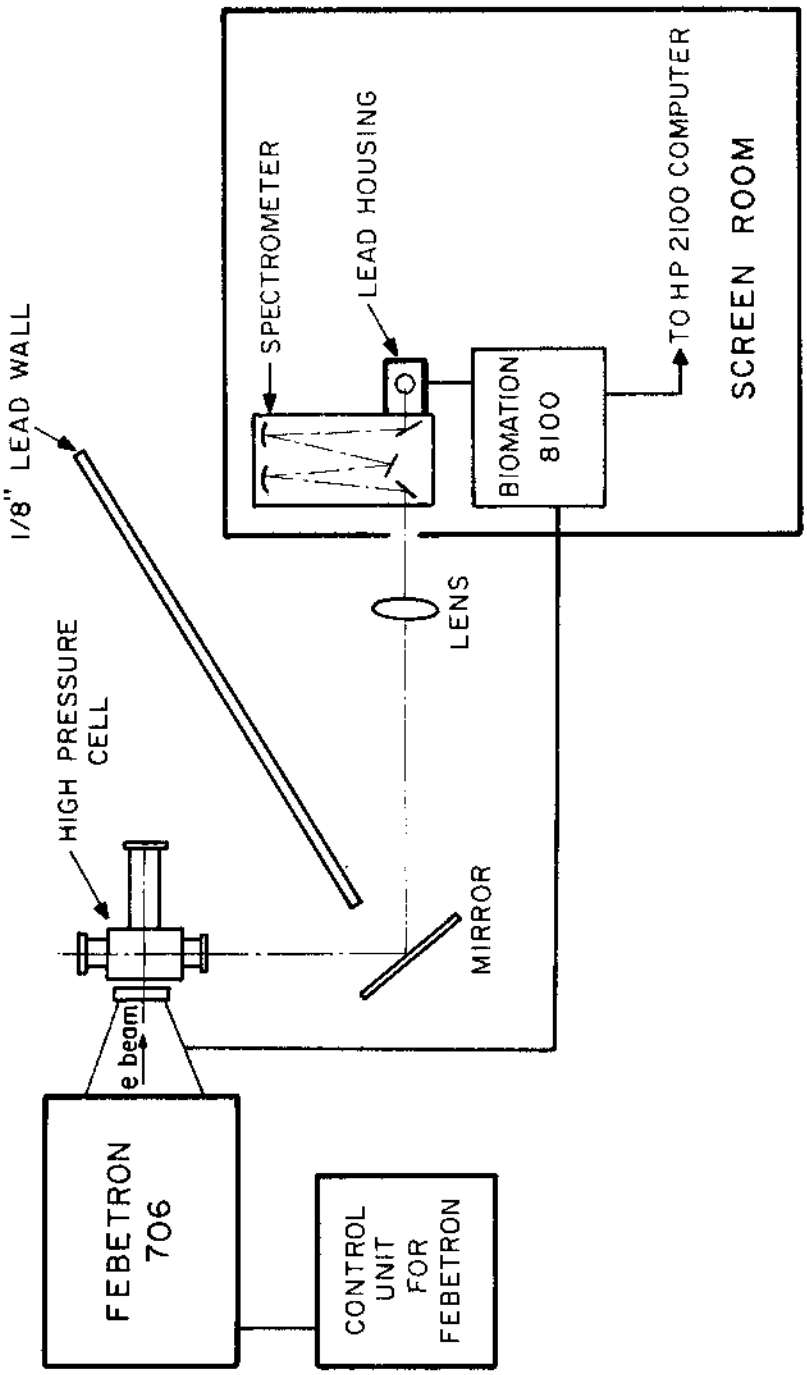

Fig. 7--Schematic representation of the arrangement of the apparatus for time resolved spectral intensities.

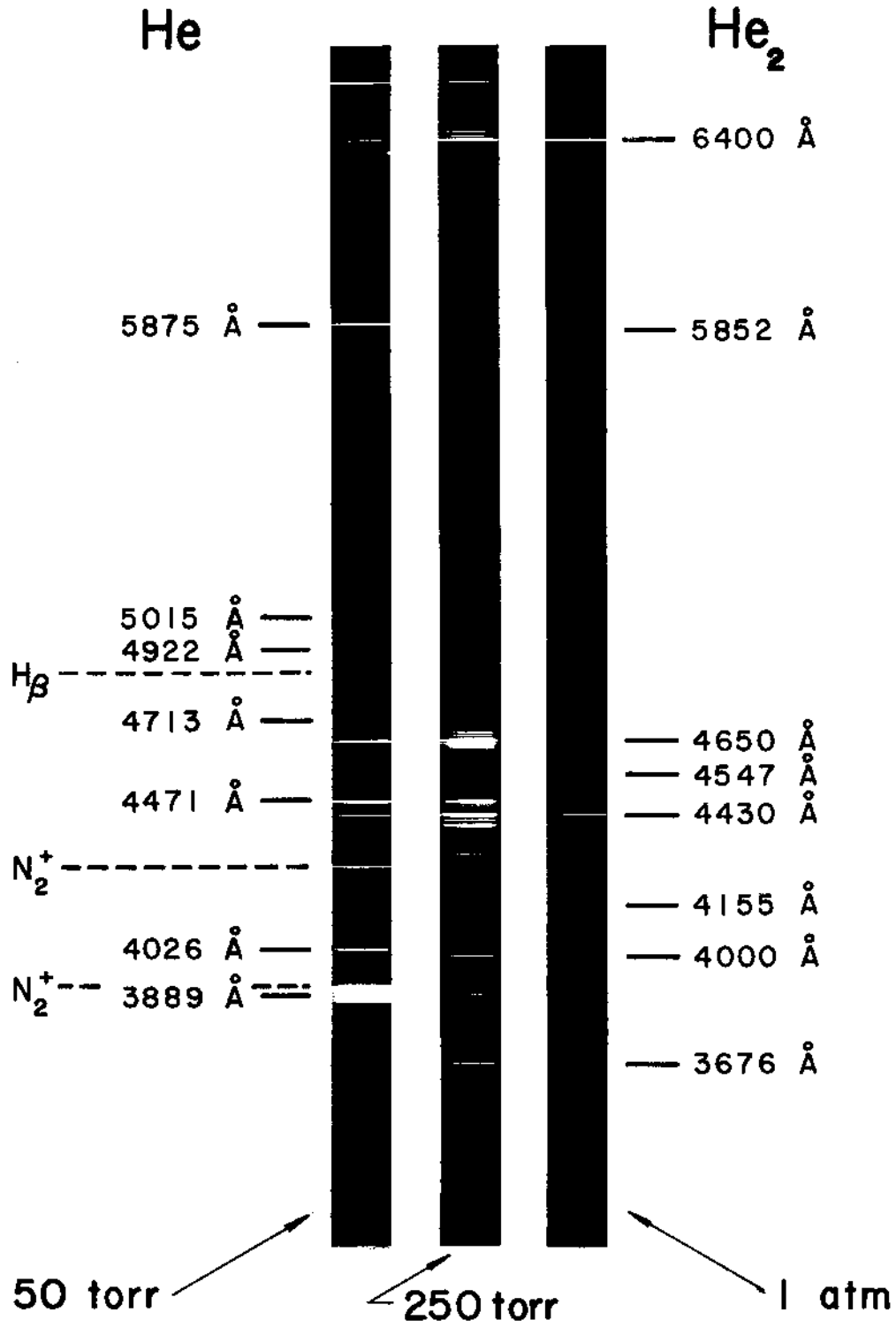

Fig. 8--Survey spectrum of the afterglows of discharges into pure helium at the three different pressures shown.

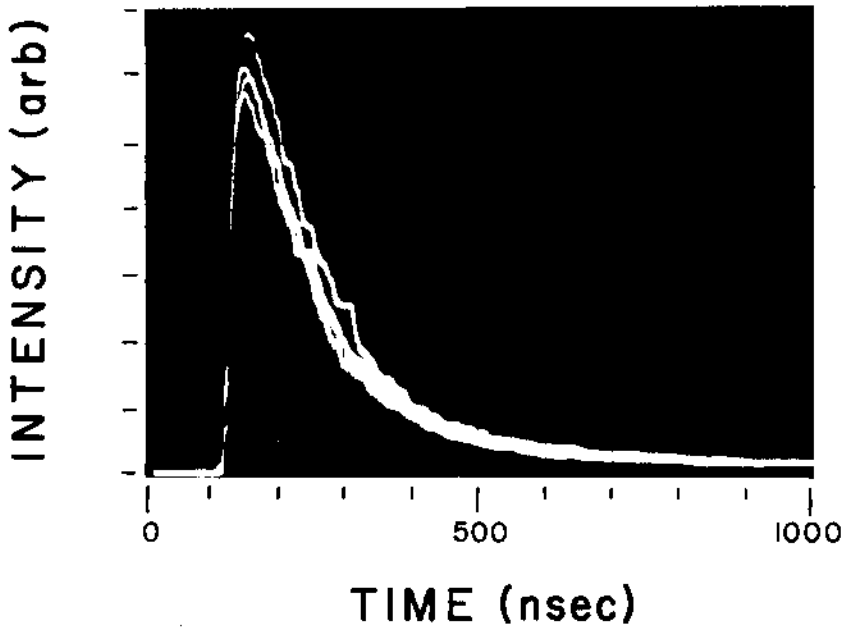

Fig. 9--Time evolution of four successive pulsed excitations of the 4278 Å in the electron-beam afterglow at one atmosphere helium with 150 μ Hg of nitrogen.

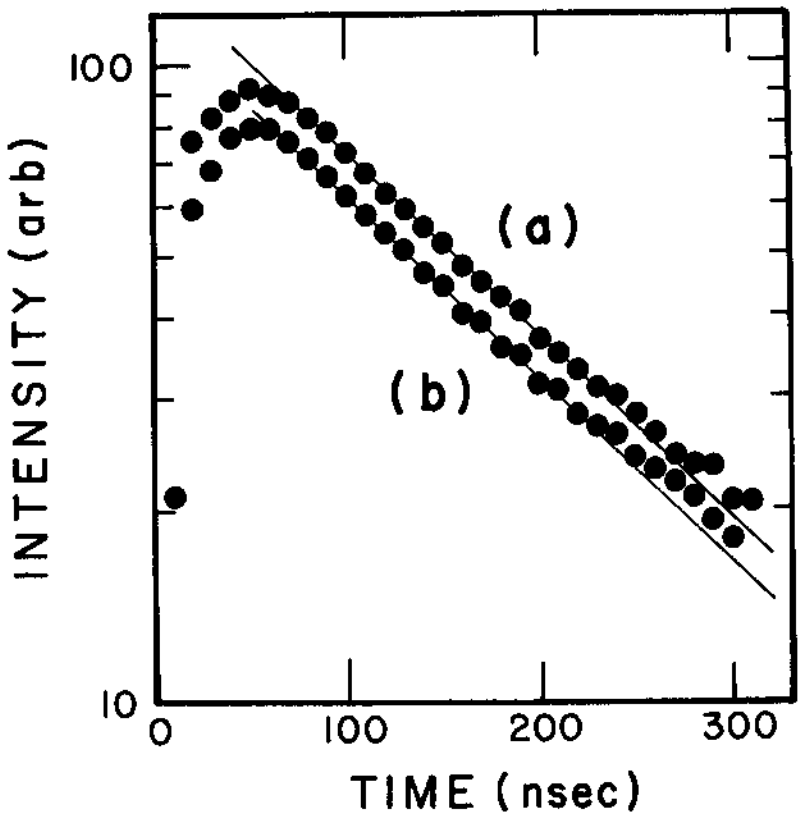

Fig. 10--Graph of the decay of the logarithm of the intensity of the spontaneous emission detected at 4278 Å as a function of time at a pressure of 818 torr helium containing 100 μ Hg nitrogen. (a): Signal detected at 1 volt full scale of digitization range. (b): Signal detected at 0.4 volt full scale of digitization range and attenuated with a 0.5 neutral density filter.

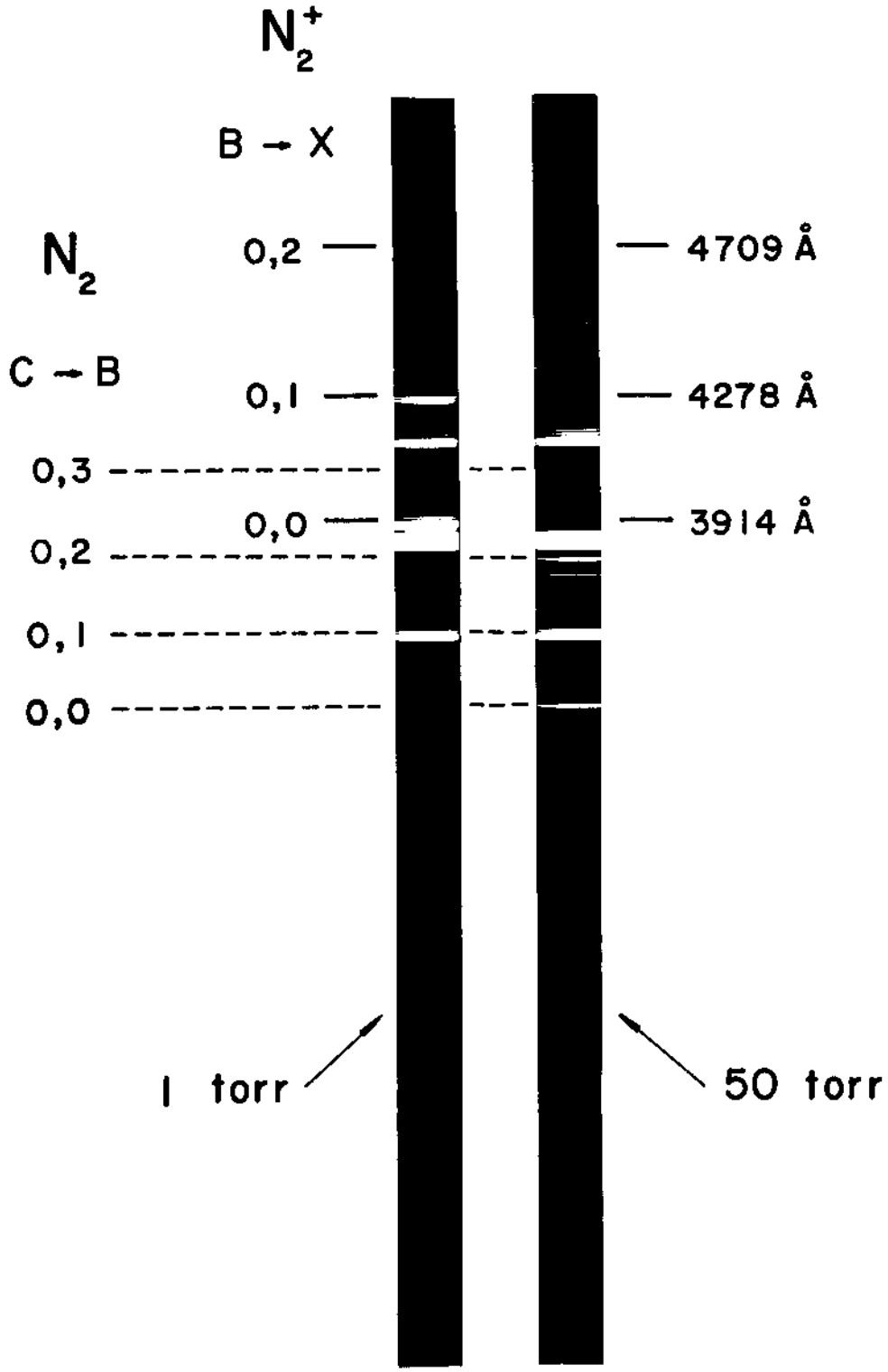

Fig. 11--Spectra of an electron-beam discharge into each of two samples of nitrogen, 1 torr and 50 torr, diluted in 1 atmosphere of helium.

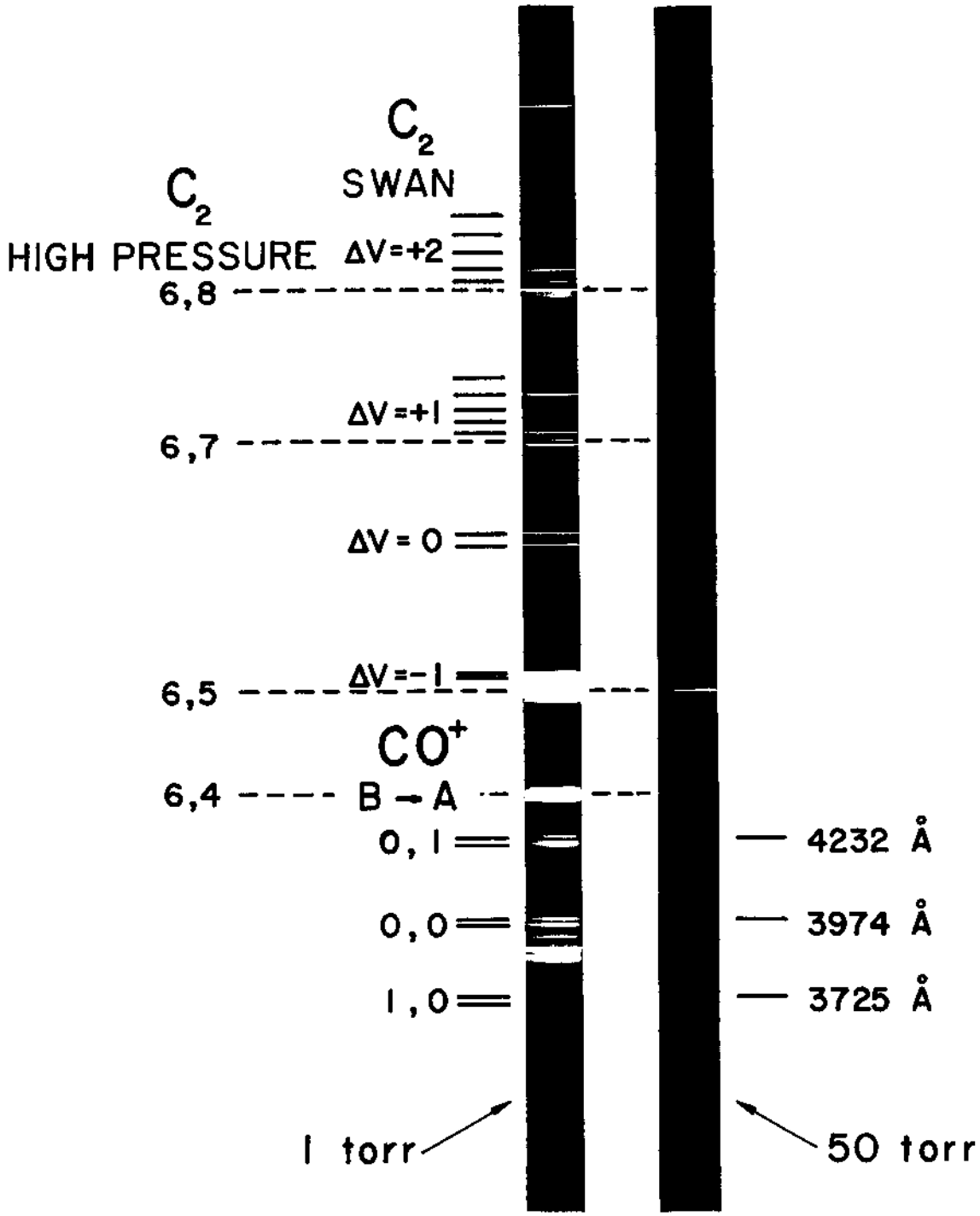

Fig. 12--Spectra of an electron-beam discharge into each of two samples of carbon monoxide, 1 torr and 50 torr, diluted in one atmosphere of helium.

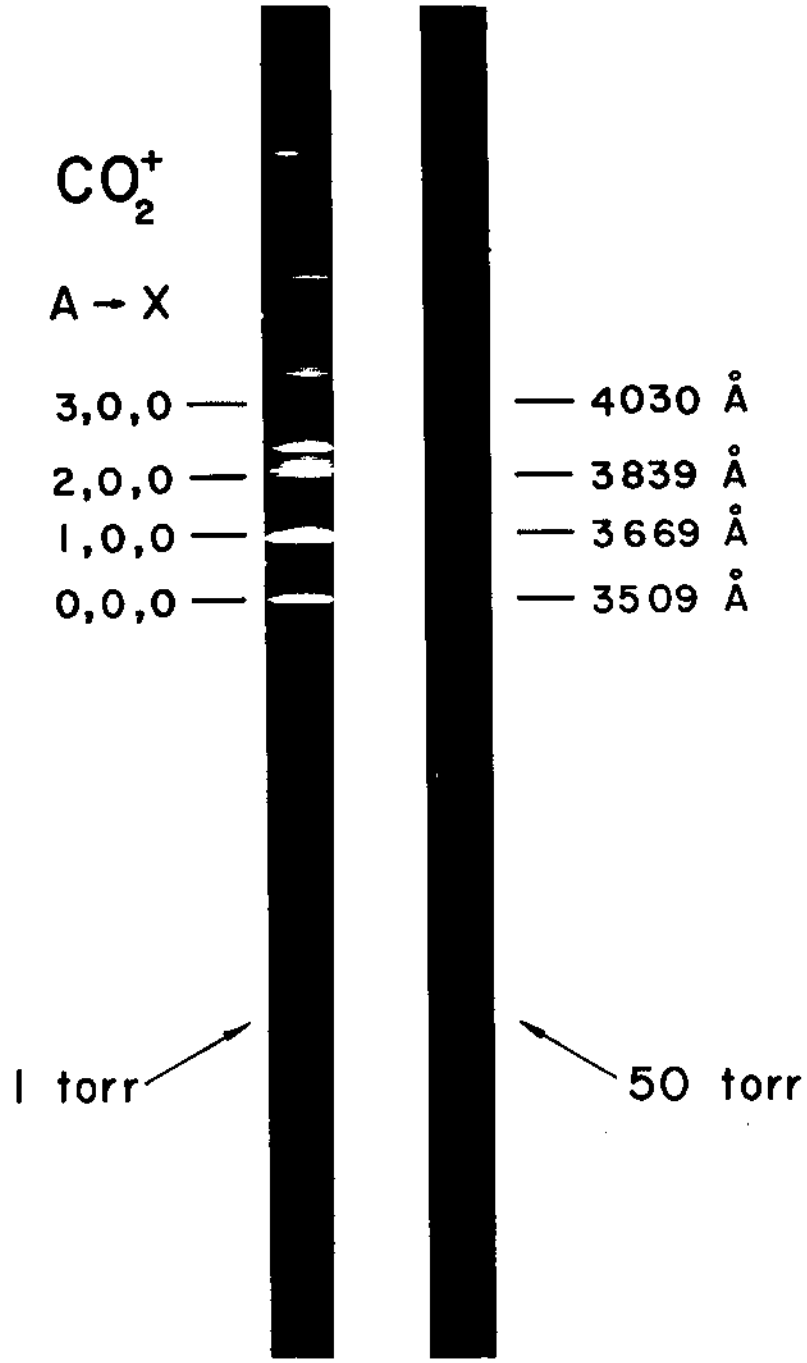

Fig. 13--Spectra of an electron-beam discharge into each of two samples of carbon dioxide, 1 torr and 50 torr, diluted in one atmosphere of helium.

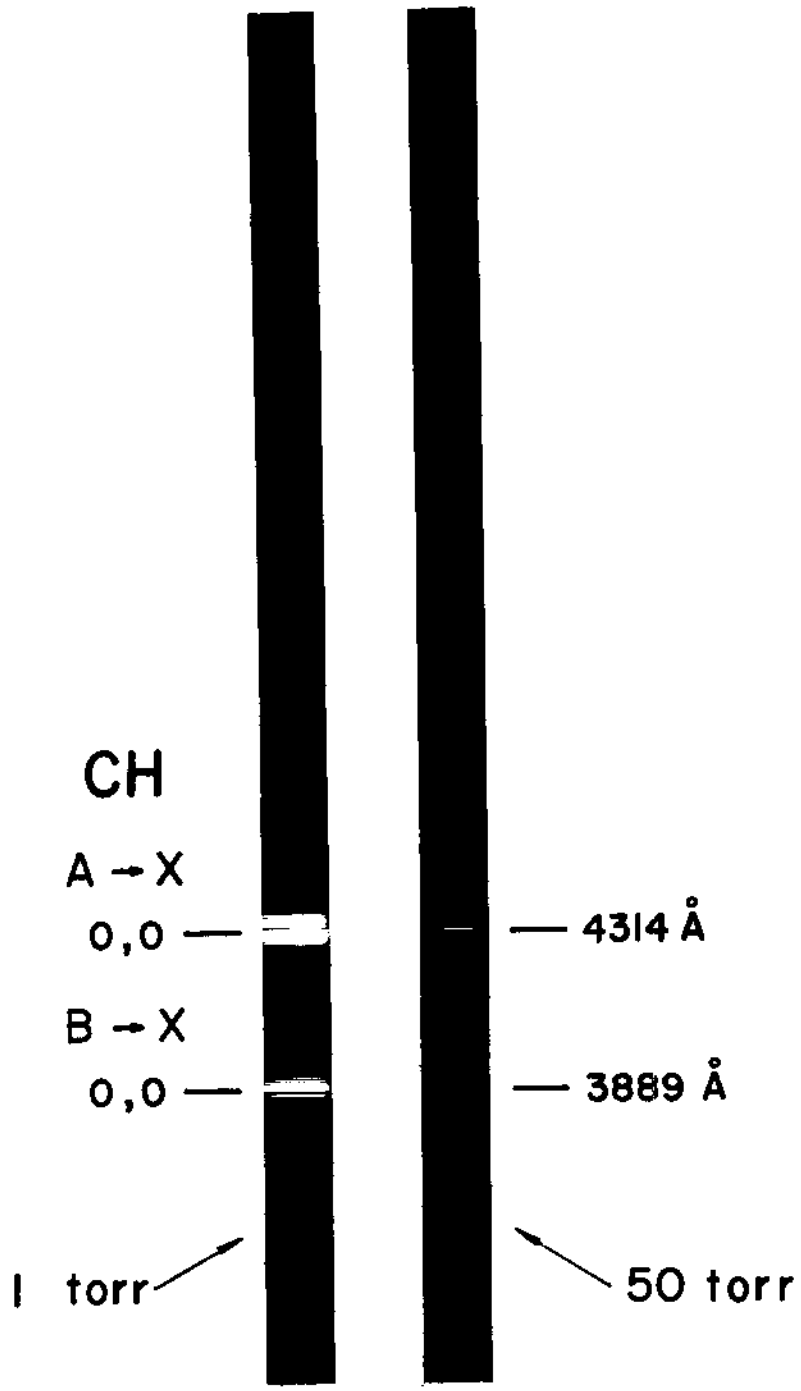

Fig. 14--Spectra of an electron-beam discharge into each of two samples of methane, 1 torr and 50 torr, diluted in one atmosphere of helium.

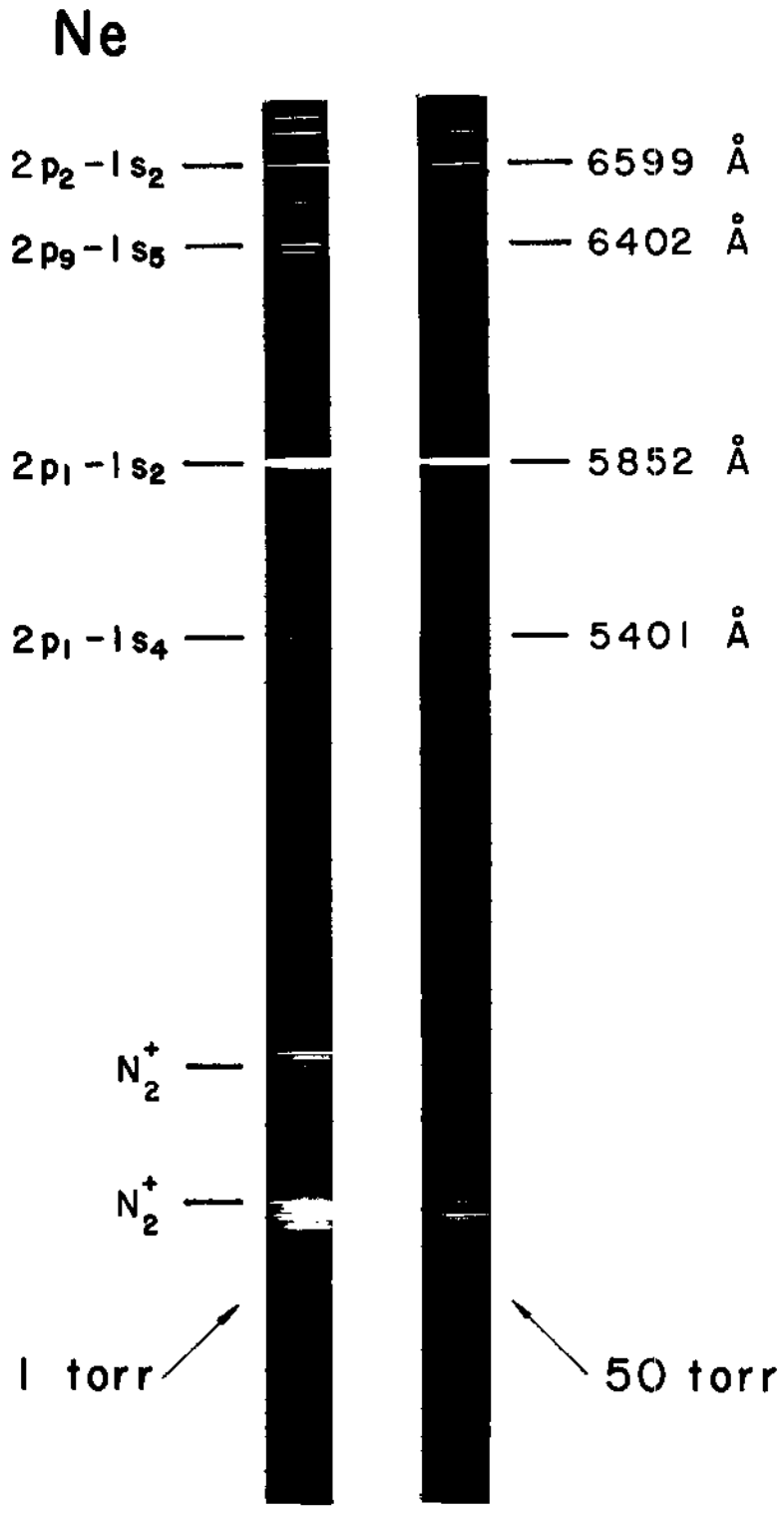

Fig. 15--Spectra of an electron-beam discharge into each of two samples of neon, 1 torr and 50 torr, diluted in 1 atmosphere of helium.

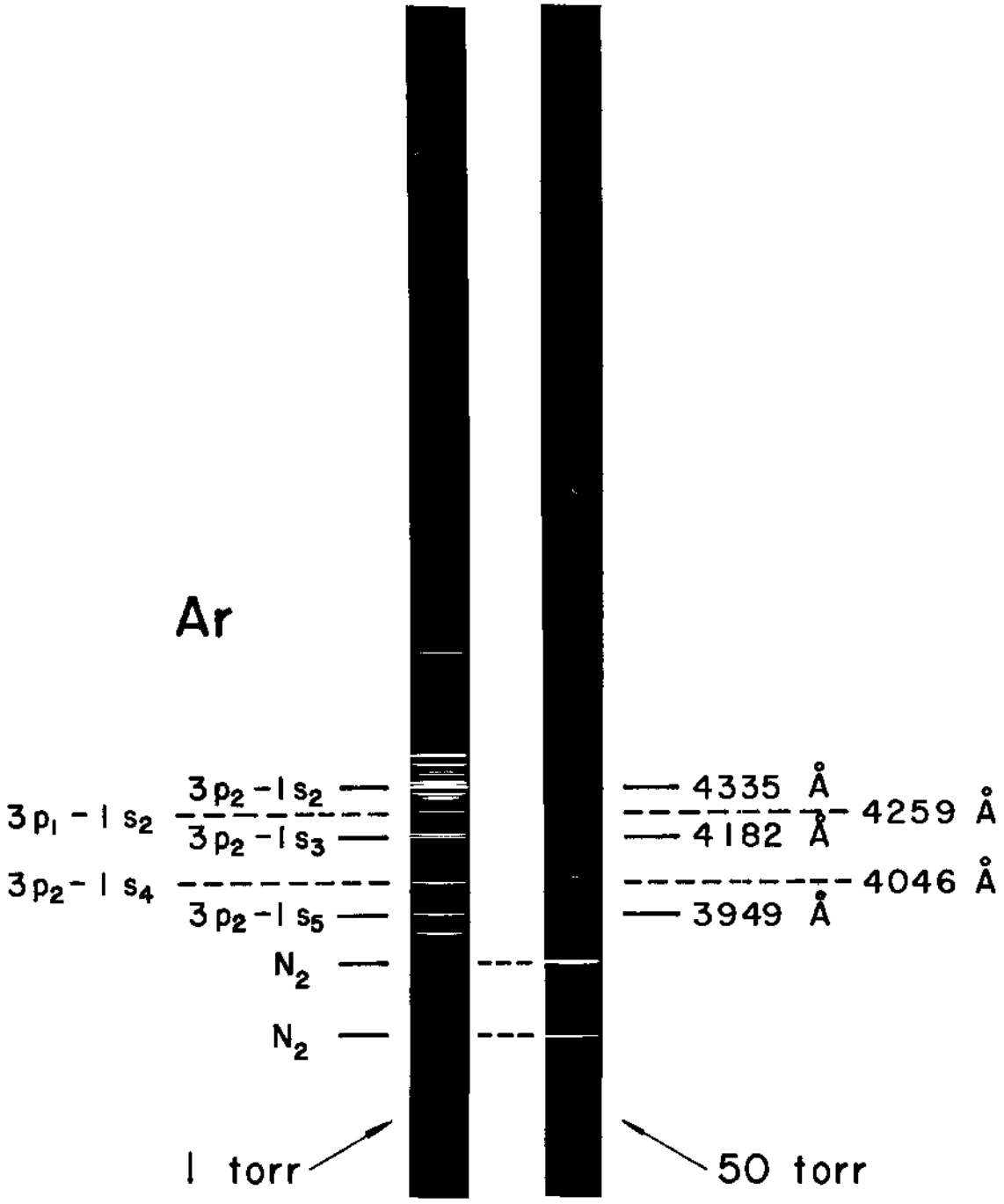

Fig. 16--Spectra of an electron-beam discharge into each of two samples of argon, 1 torr and 50 torr, diluted in 1 atmosphere of helium.

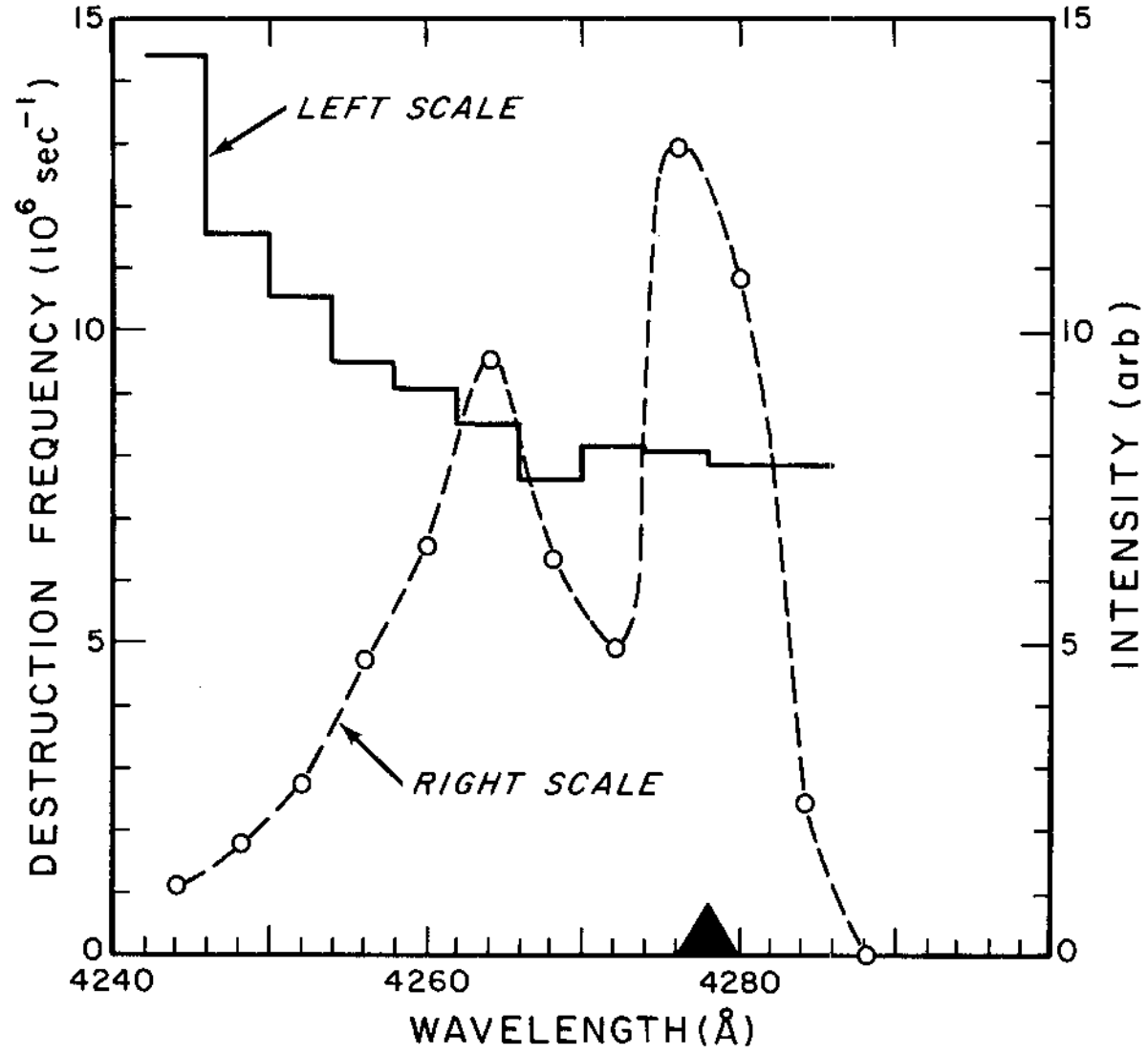

Fig. 17--Solid line: Dispersion curve as a function of wavelength of the logarithmic derivative with respect to time of the intensity of spontaneous emission from 924 torr of helium containing 200 μ Hg of nitrogen. Dashed curve: Peak of the transient intensity from the same gas samples measured in arbitrary units on the scale to the right as a function of wavelength. The actual spectrometer setting subsequently used to monitor the N_2^+ fluorescence is shown by the triangle immediately above the abscissa.

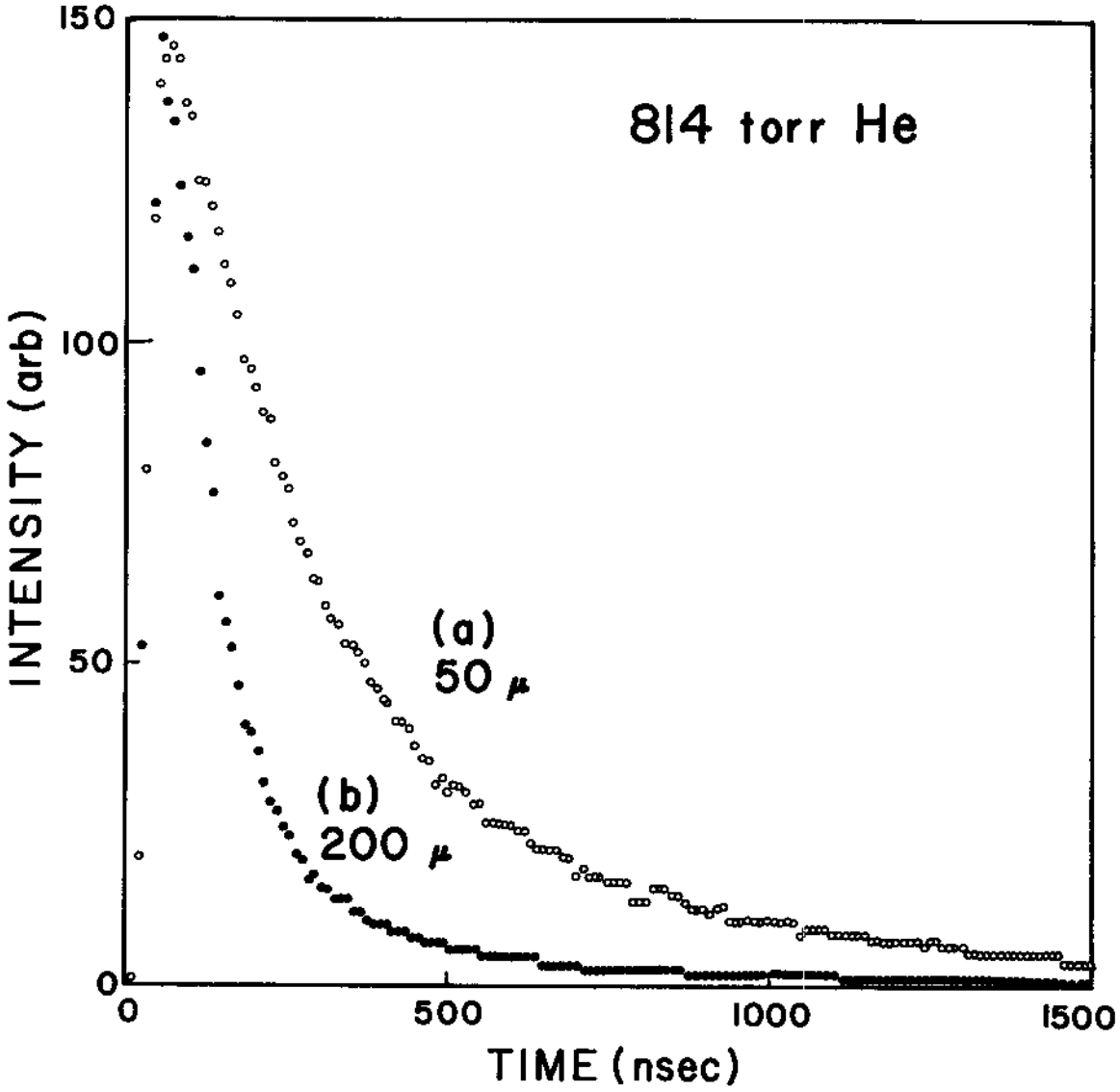

Fig. 18--Typical data for the transient dependence of the intensity emitted at 4278 Å from the afterglow of a mixture of helium and nitrogen.
(a) Experimental conditions: He-- 814 torr, N_2--50μ
(b) Experimental conditions: He-- 814 torr, N_2--200μ

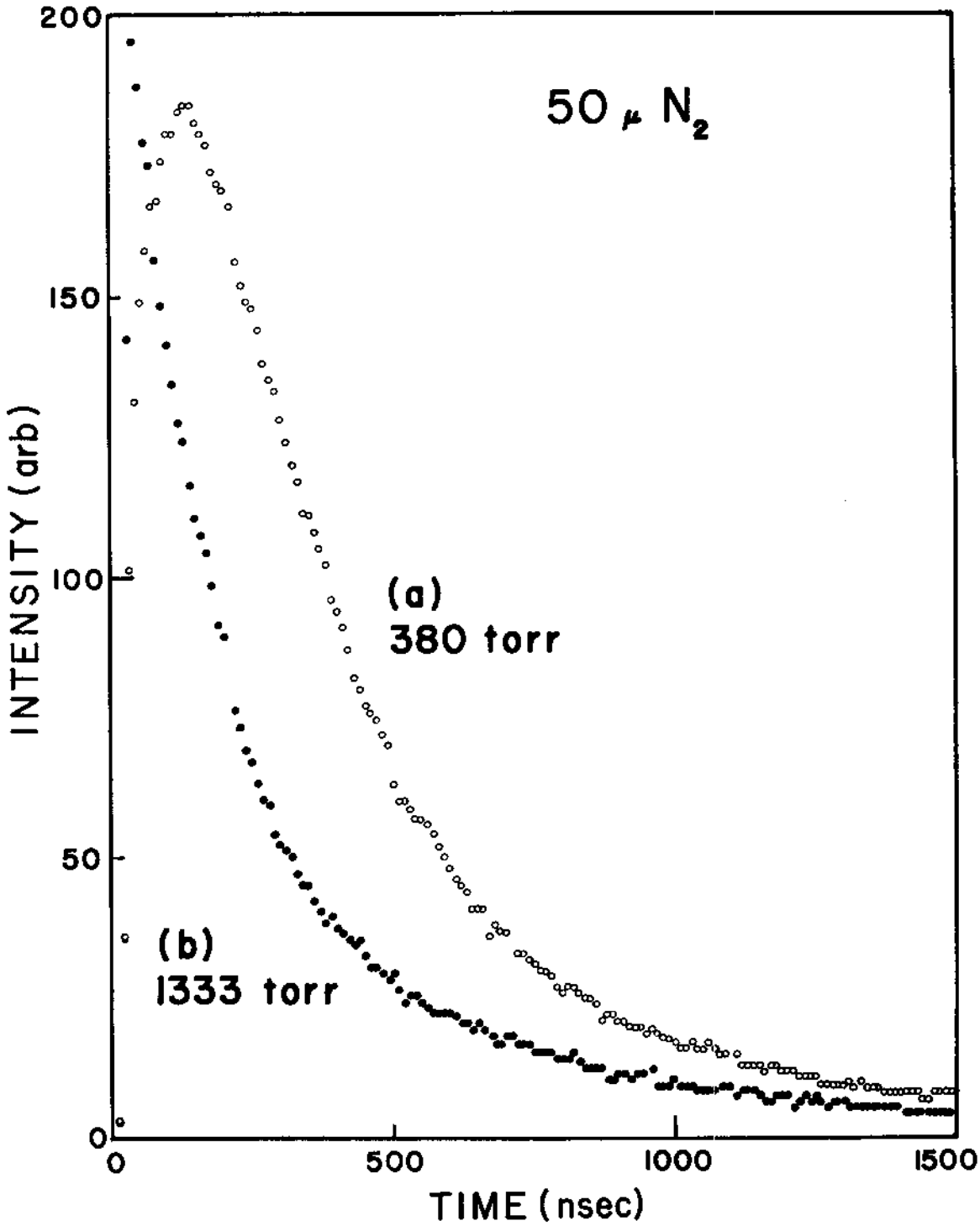

Fig. 19--Typical data for the transient dependence of the intensity emitted at 4278 Å from the afterglow of a mixture of helium and nitrogen.
(a) Experimental conditions: He--380 torr, N_2--50μ
(b) Experimental conditions: He--1333 torr, N_2--50μ

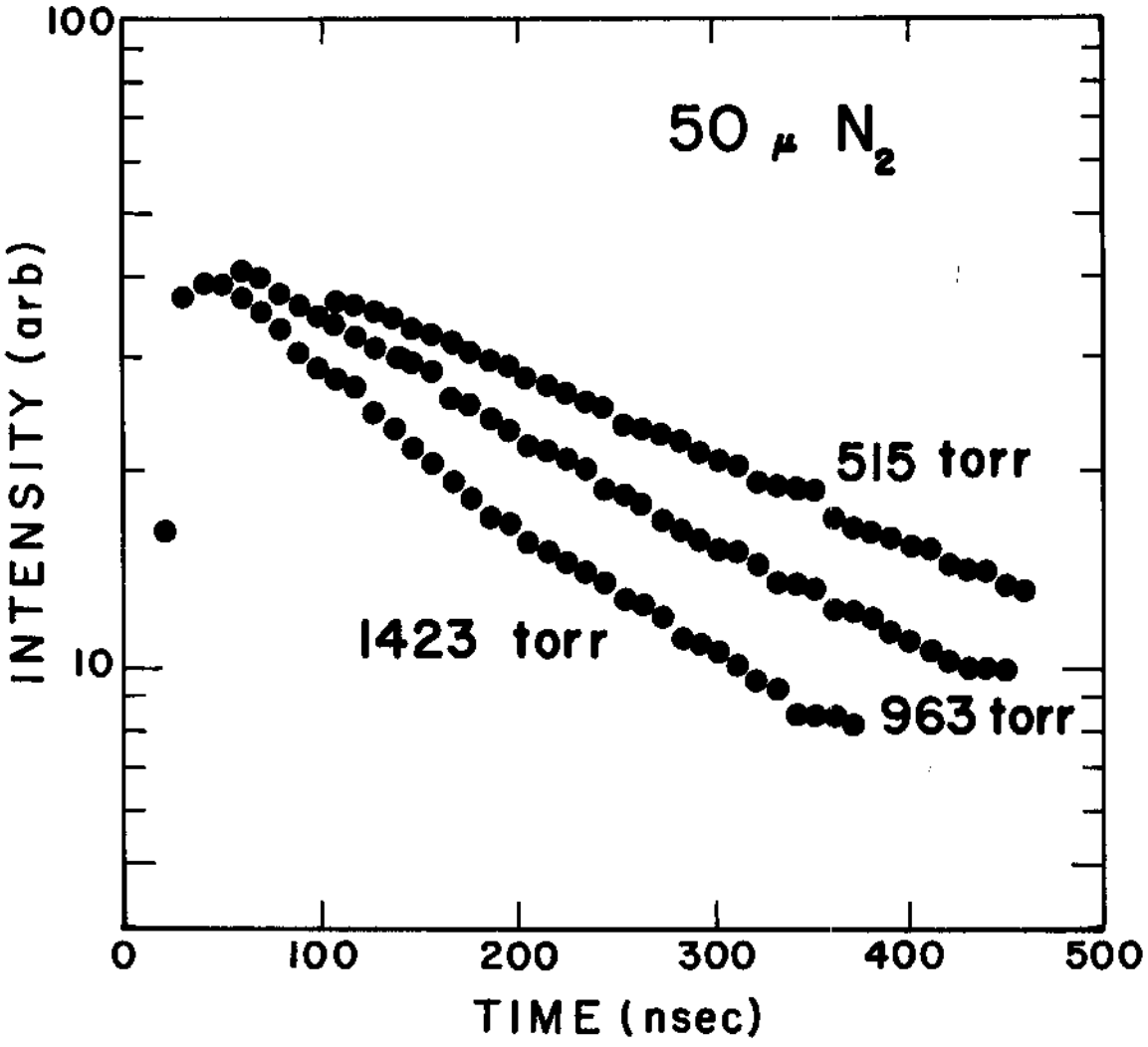

Fig. 20--Typical data for the transient dependence of the intensity at 4278 Å from the afterglow of 50 μ Hg partial pressure of nitrogen diluted into the different pressures of helium.

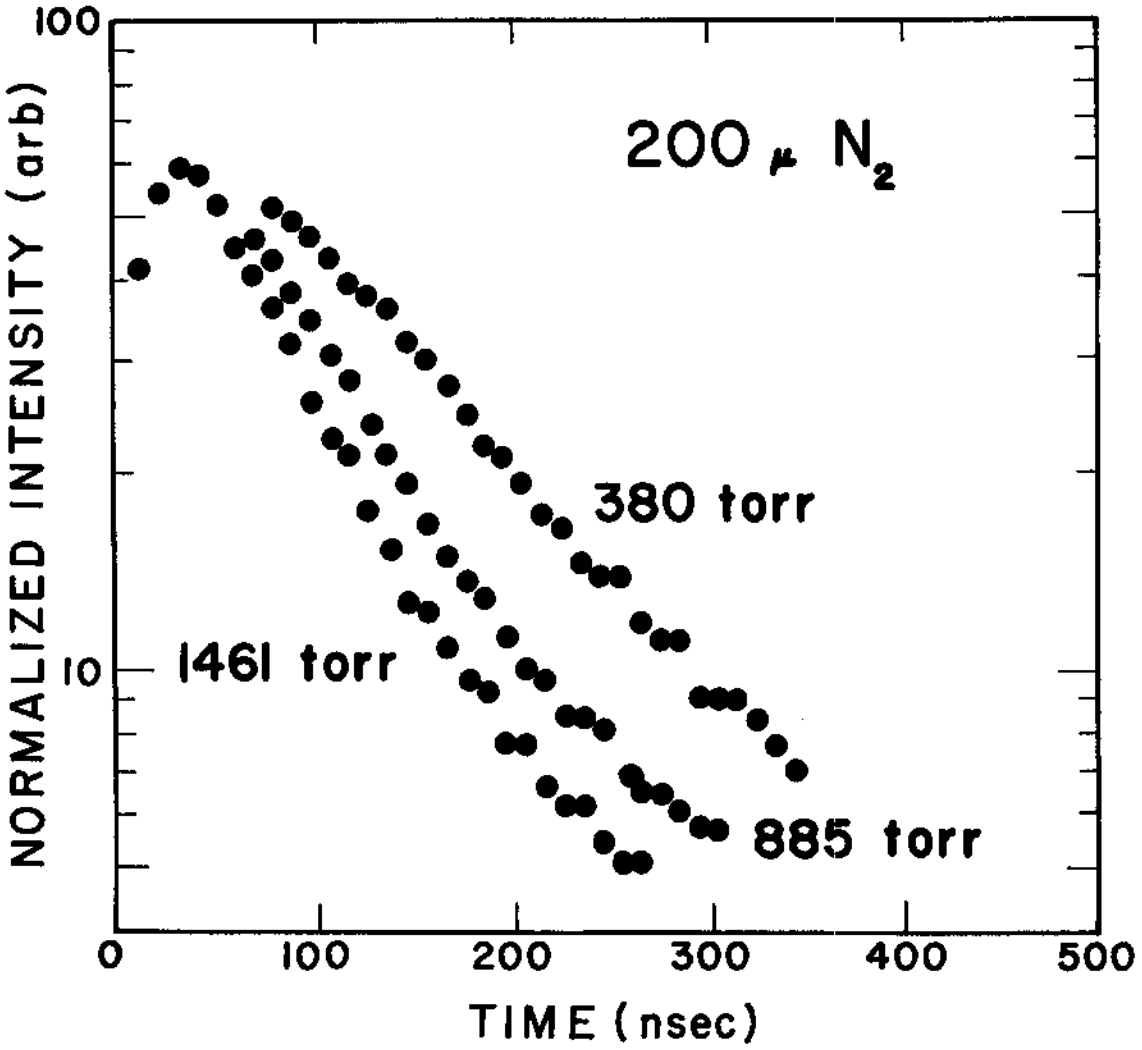

Fig. 21--Typical data for the transient dependence of the intensity at 4278 Å from the afterglow of 200 μ Hg partial pressure of nitrogen diluted into the different pressures of helium.

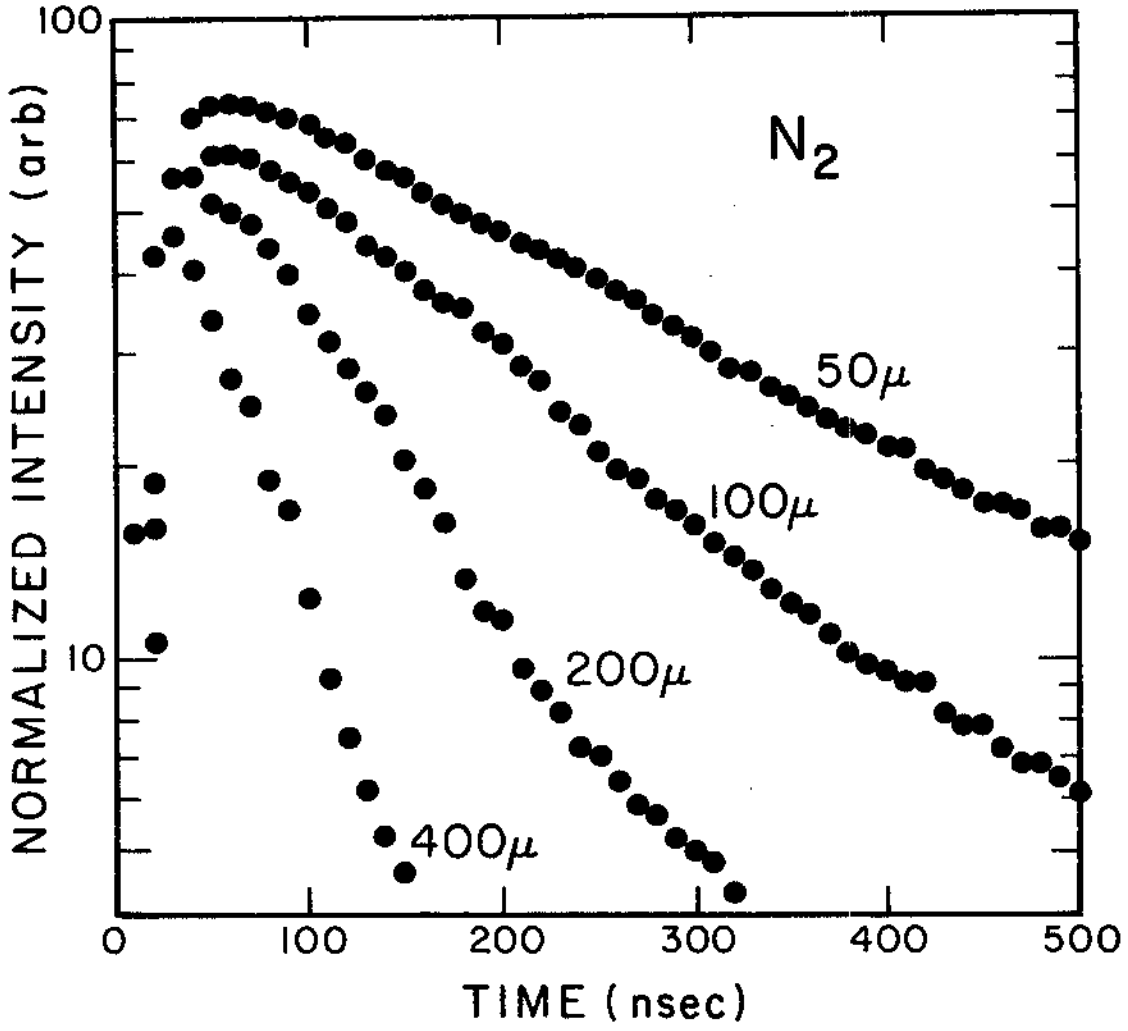

Fig. 22--Graphs of the transient intensity at 4278 Å measured in the afterglow of an intense electron beam discharge into 830 torr of helium containing the indicated partial pressures of nitrogen.

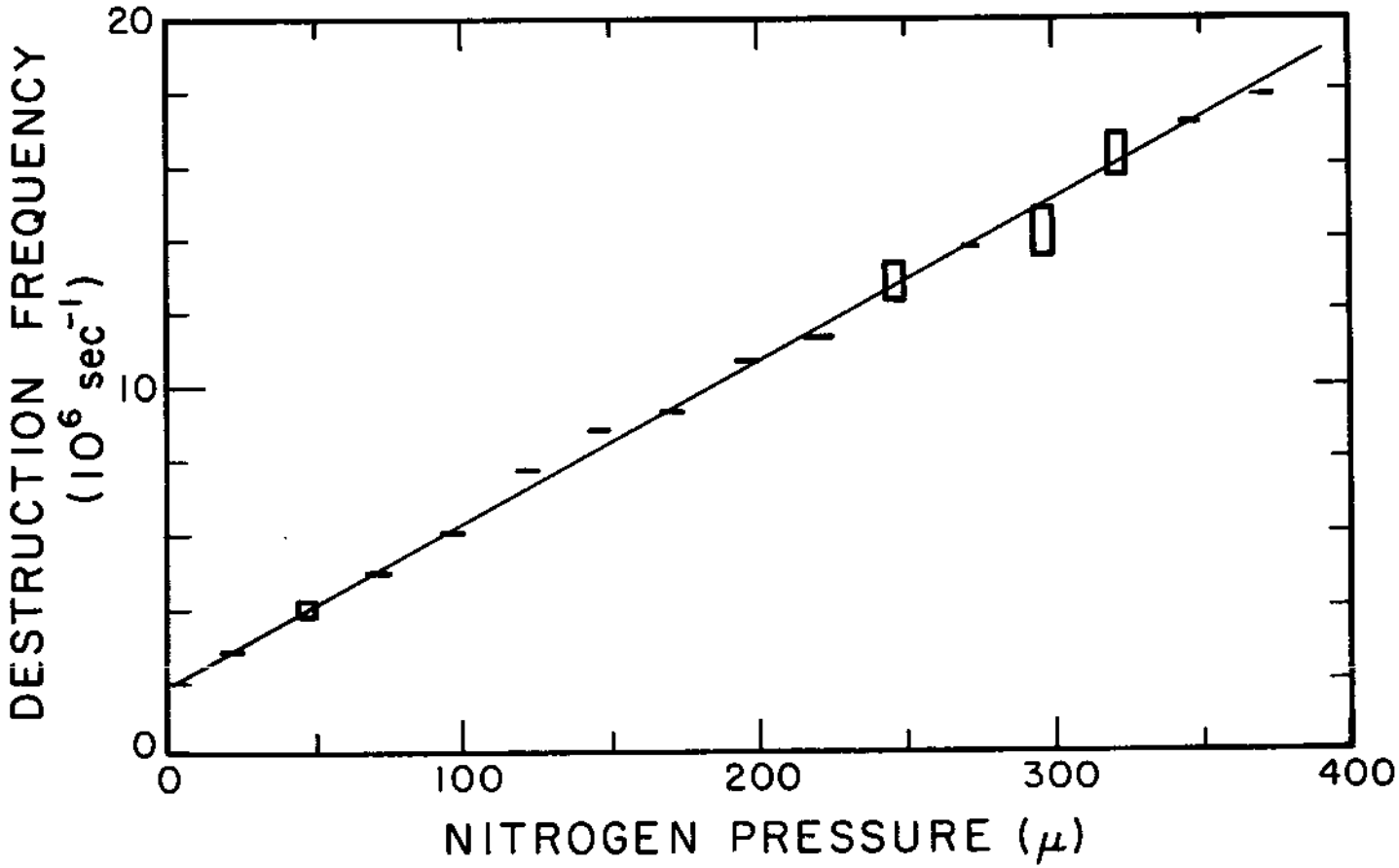

Fig. 23--Stern-Volmer plot of the destruction frequency of the exponential decay of the intensity at 4278 Å as a function of the partial pressure of nitrogen added to 830 torr of helium.

Fig. 24--Graph of the measured destruction frequencies of the transient intensities of transitions to two different lower states from product $N_2^+(B^2\Sigma_u)$ molecules resulting from the charge transfer from He_2^+ as functions of helium pressure in the afterglow of an intense electron beam discharge. The type of symbol indicates the corresponding wavelength; (0) 4278 Å ; (+) 3914 Å. Partial pressures of nitrogen are indicated and comparison values of ν computed from Eq. (5.4) using previously reported bimolecular rate coefficients are shown together with the reported experimental uncertainty where available.

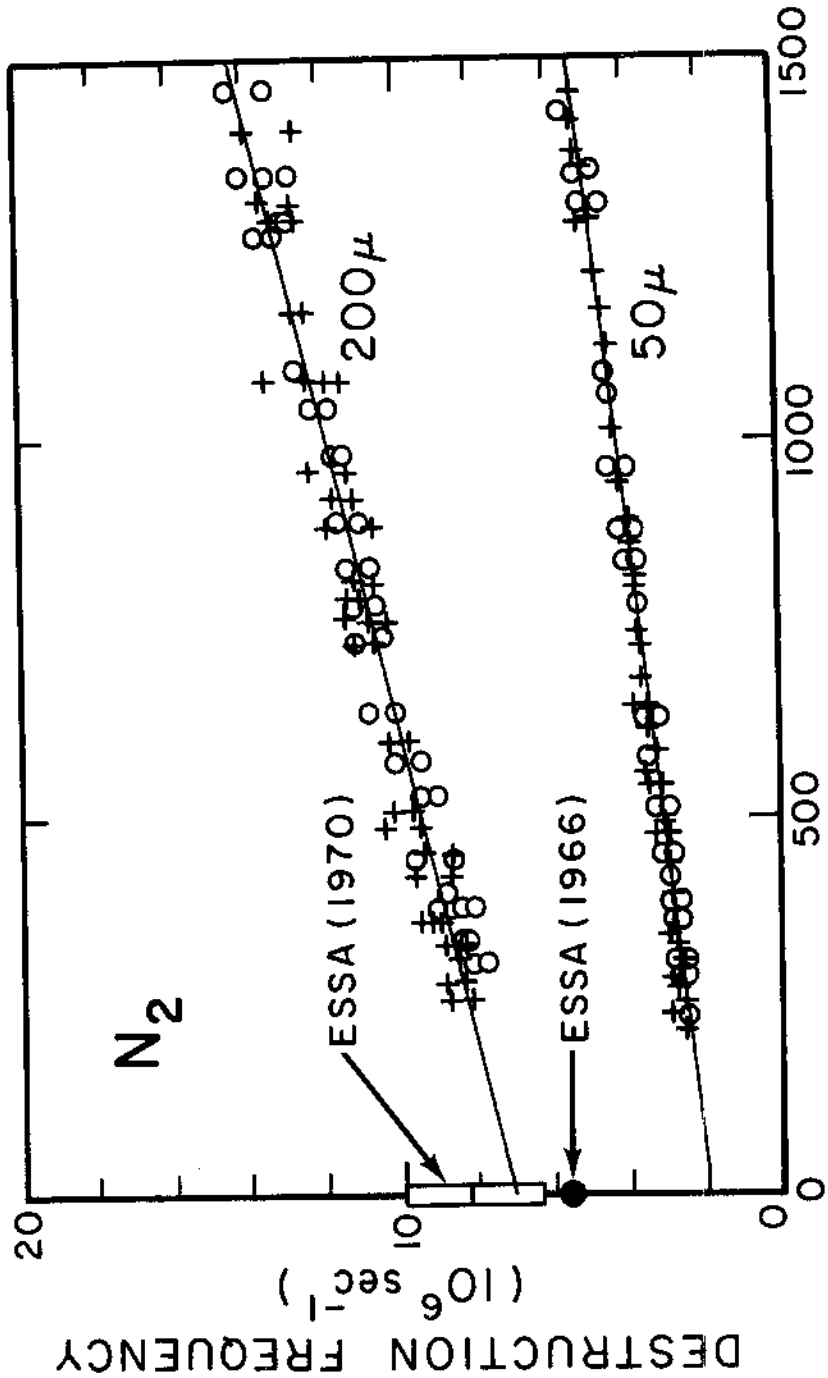
DESTRUCTION FREQUENCY
(10^6 sec^{-1})
20
10
0
0
500
1000
1500
HELIUM PRESSURE (torr.)
N_2
ESSA (1970)
ESSA (1966)
200μ
50μ

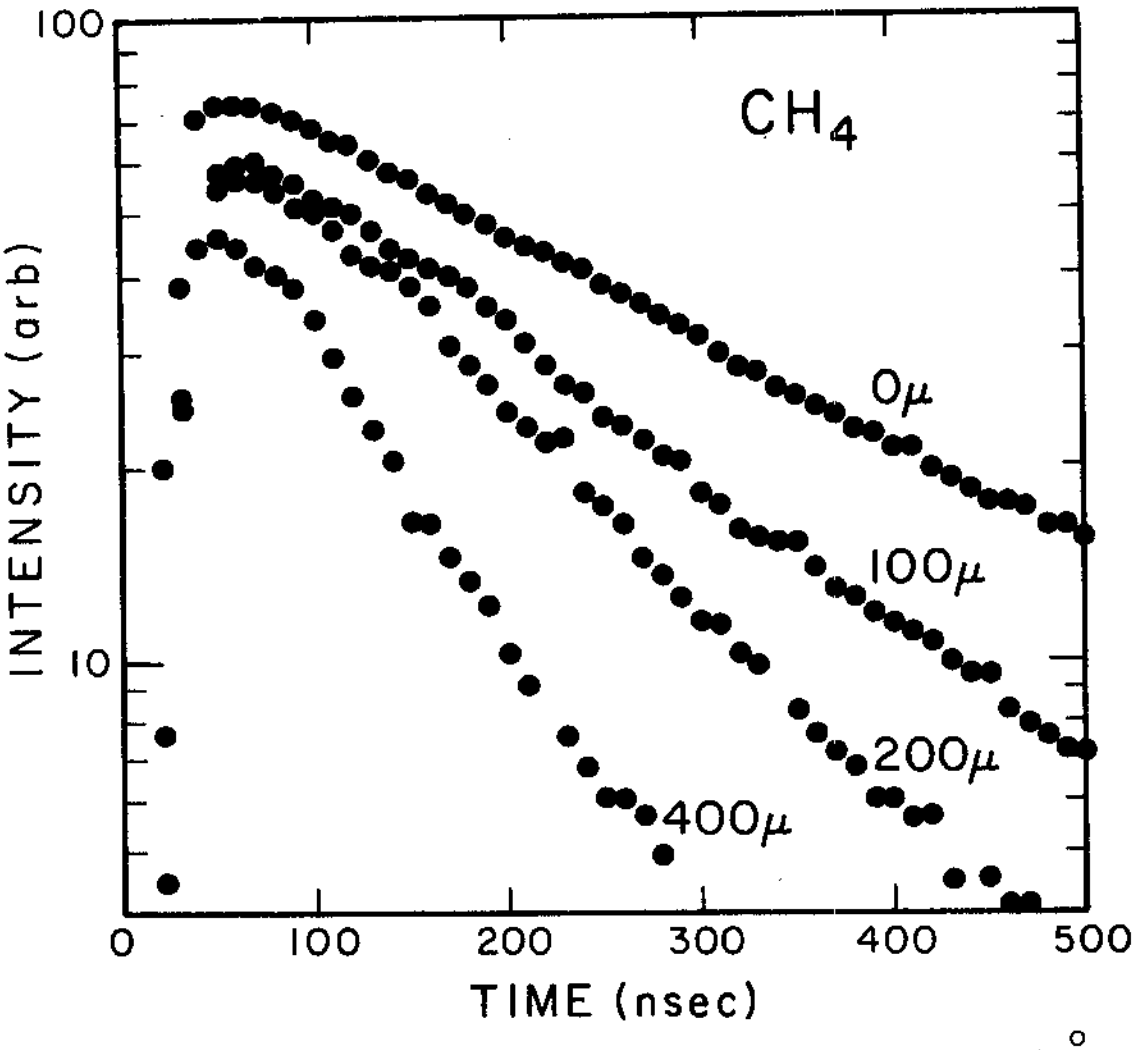

Fig. 25--Graphs of the transient intensity at 4278 Å from the 50 μ Hg admixture of N_2 used to monitor the He_2^+ concentration as functions of time in the 770 torr helium afterglow containing the indicated partial pressures of CH_4 reactant.

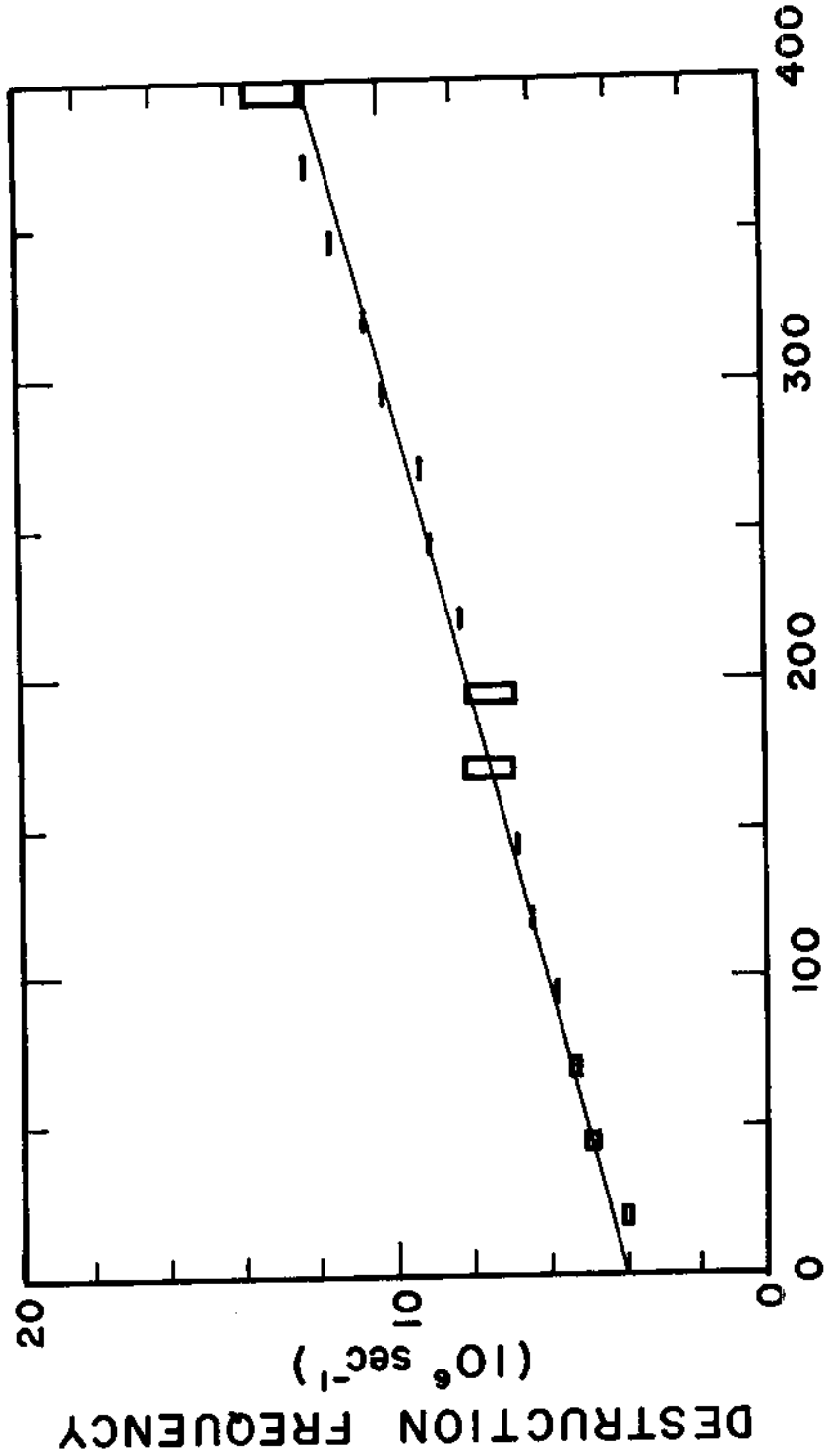

Fig. 26--Stern-Volmer plot of the destruction frequency of the exponential decay of the intensity at 4278 Å from the 50 μ Hg of nitrogen used to monitor the He_2^+ concentration as a function of the partial pressure of methane added to 770 torr of helium.

Fig. 27--Graphs as functions of helium pressure of the measured destruction frequencies of the transient intensities of 4278 Å radiation from the 50 μ Hg of nitrogen used to monitor the time dependence of the He_2^+ concentration. Partial pressures of the added CH_4 reactant are indicated. Linear approximations are shown which best fit the data while remaining consistent with Eq. (5.5). The dashed line records base conditions of destruction frequency in the absence of the added reactant obtained from the 50 μ Hg nitrogen data of Fig. 24, and filled circles record agreement of subsequent remeasurements performed at the end of the data set shown.

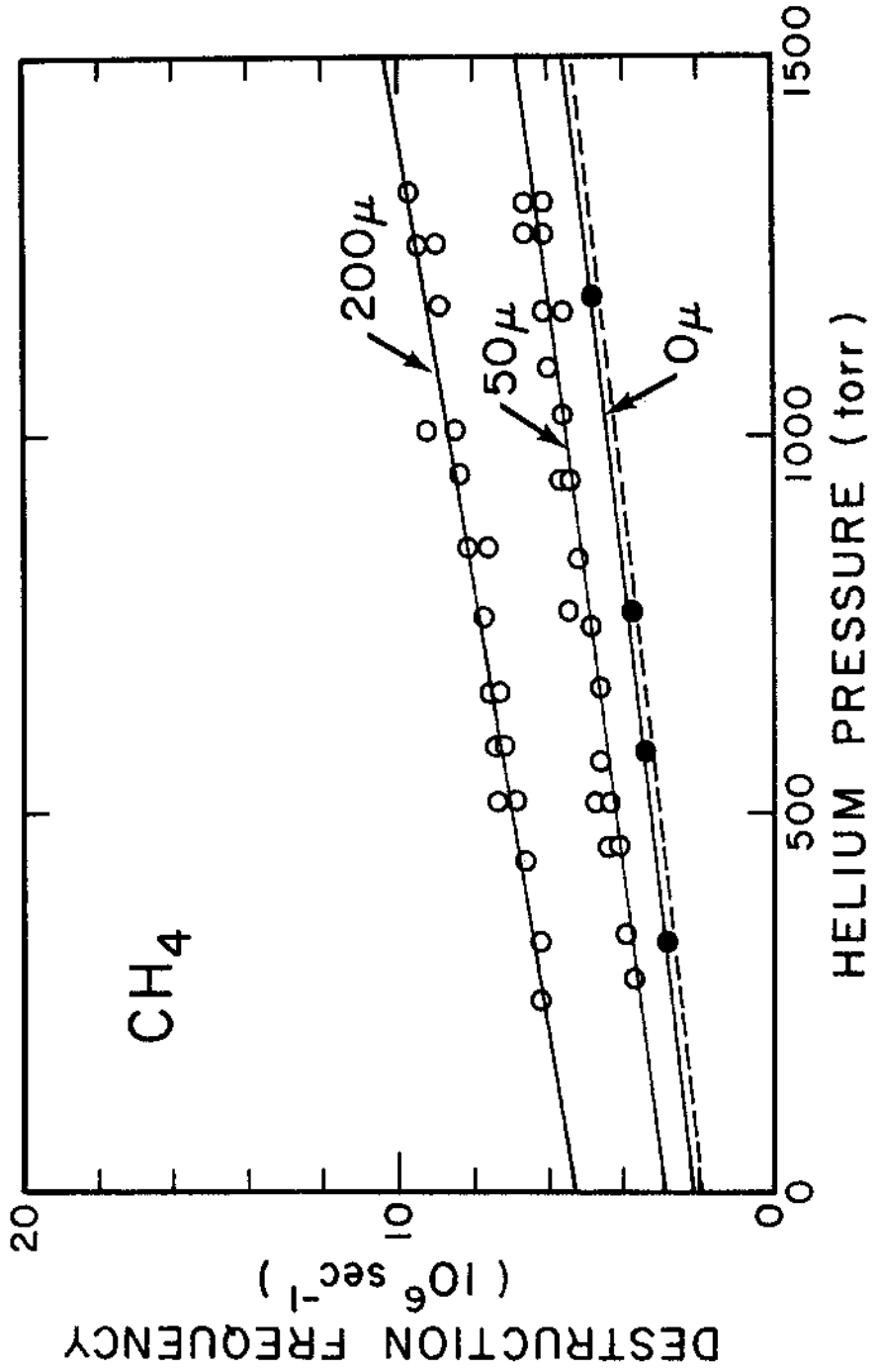
DESTRUCTION FREQUENCY
(10^6 sec^{-1})
20
10
0
0
500
1000
1500
HELIUM PRESSURE (torr)
CH_4
200μ
50μ
0μ

Fig. 28--Graphs as functions of helium pressure of the measured destruction frequencies of the transient intensities of 4278 Å radiation from the 50 μ Hg of nitrogen used to monitor the time dependence of the He_2^+ concentration. Partial pressures of the added Ne reactant are indicated and comparison values of ν computed from Eq. (5.4) using previously reported bimolecular rate coefficients are shown together with the reported experimental uncertainty. Linear approximations are shown which best fit the data while remaining consistent with Eq. (5.5). The dashed line records base conditions of destruction frequency in the absence of the added reactant obtained from the 50 μ Hg nitrogen data of Fig. 24, and filled circles record agreement of subsequent remeasurements performed at the end of the data set shown.

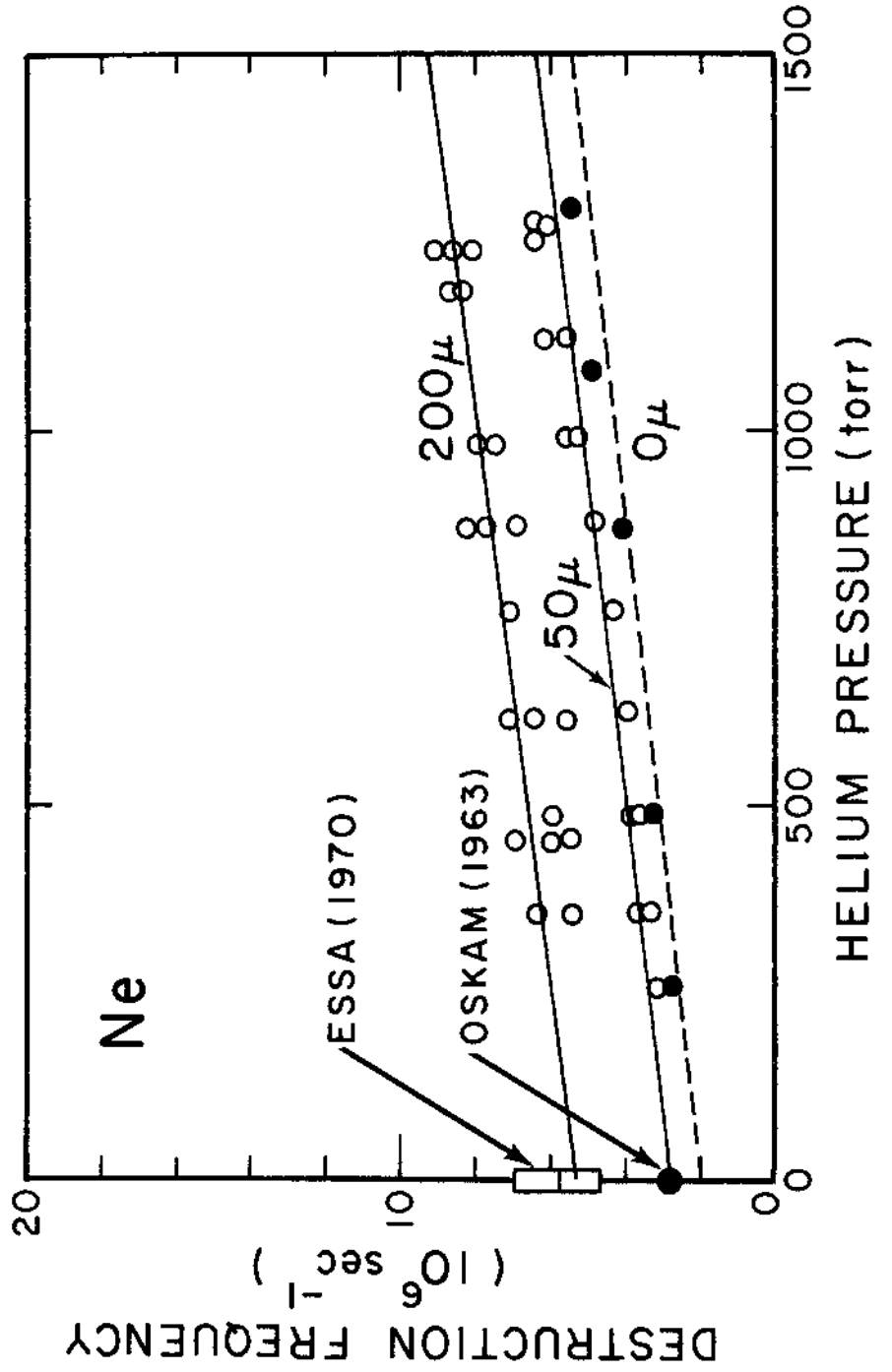
Ne
ESSA (1970)
OSKAM (1963)
200μ
50μ
0μ
DESTRUCTION FREQUENCY
(10^6 sec^-1)
HELIUM PRESSURE (torr)
0
10
20
0
500
1000
1500

Fig. 29--Graphs as functions of helium pressure of the measured destruction frequencies of the transient intensities of 4278 Å radiation from the 50 μ Hg of nitrogen used to monitor the time dependence of the He_2^+ concentration. Partial pressures of the added Ar reactant are indicated and comparison values of ν computed from Eq. (5.4) using previously reported bimolecular rate coefficients are shown together with the reported experimental uncertainty. Linear approximations are shown which best fit the data while remaining consistent with Eq. (5.5). The dashed line records base conditions of destruction frequency in the absence of the added reactant obtained from the 50 μ Hg nitrogen data of Fig. 24, and filled circles record agreement of subsequent remeasurements performed at the end of the data set shown.

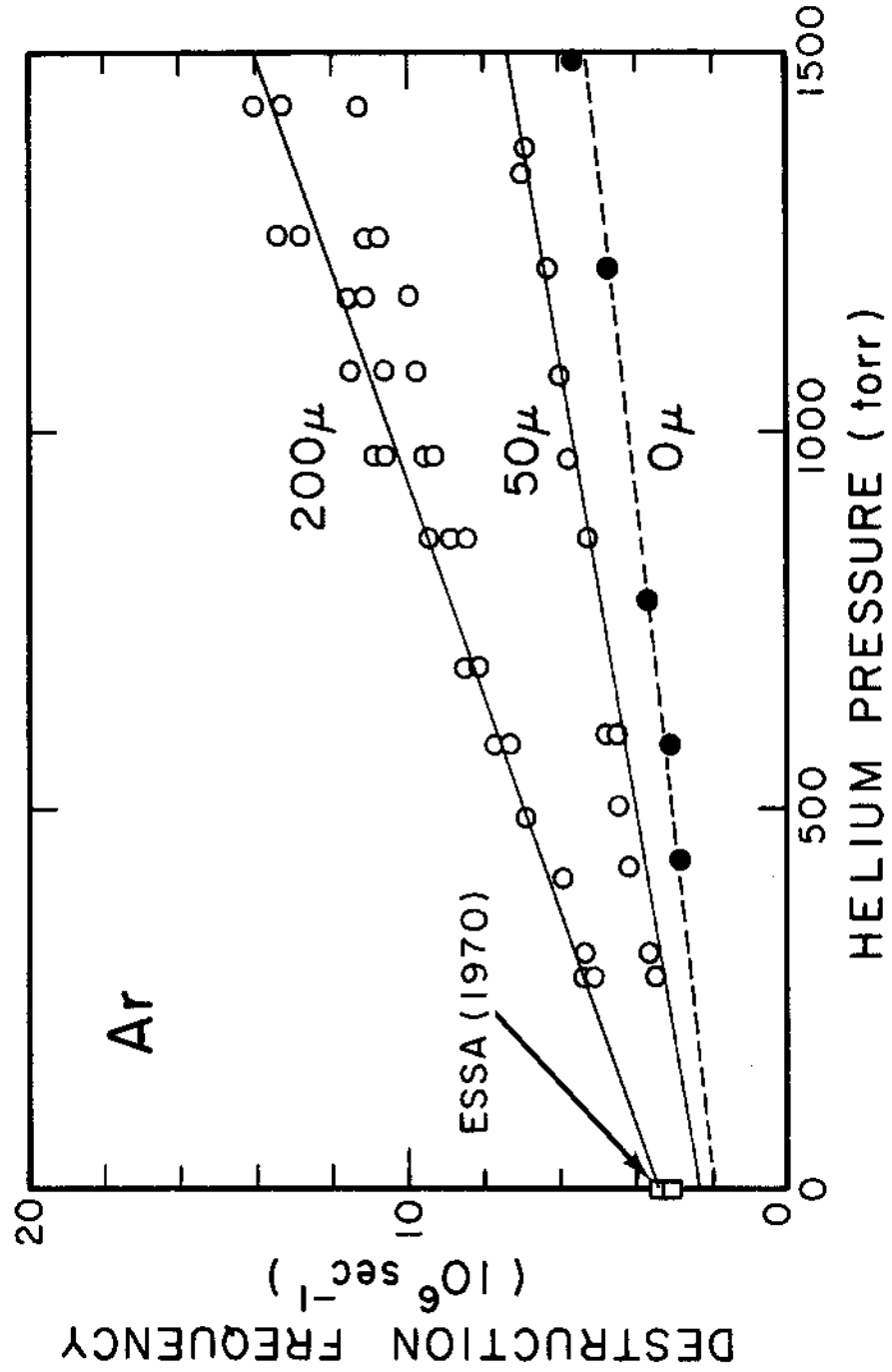
Ar
200μ
50μ
0μ
ESSA (1970)
DESTRUCTION FREQUENCY
(10^6 sec^-1)
HELIUM PRESSURE (torr)
0
10
20
0
500
1000
1500

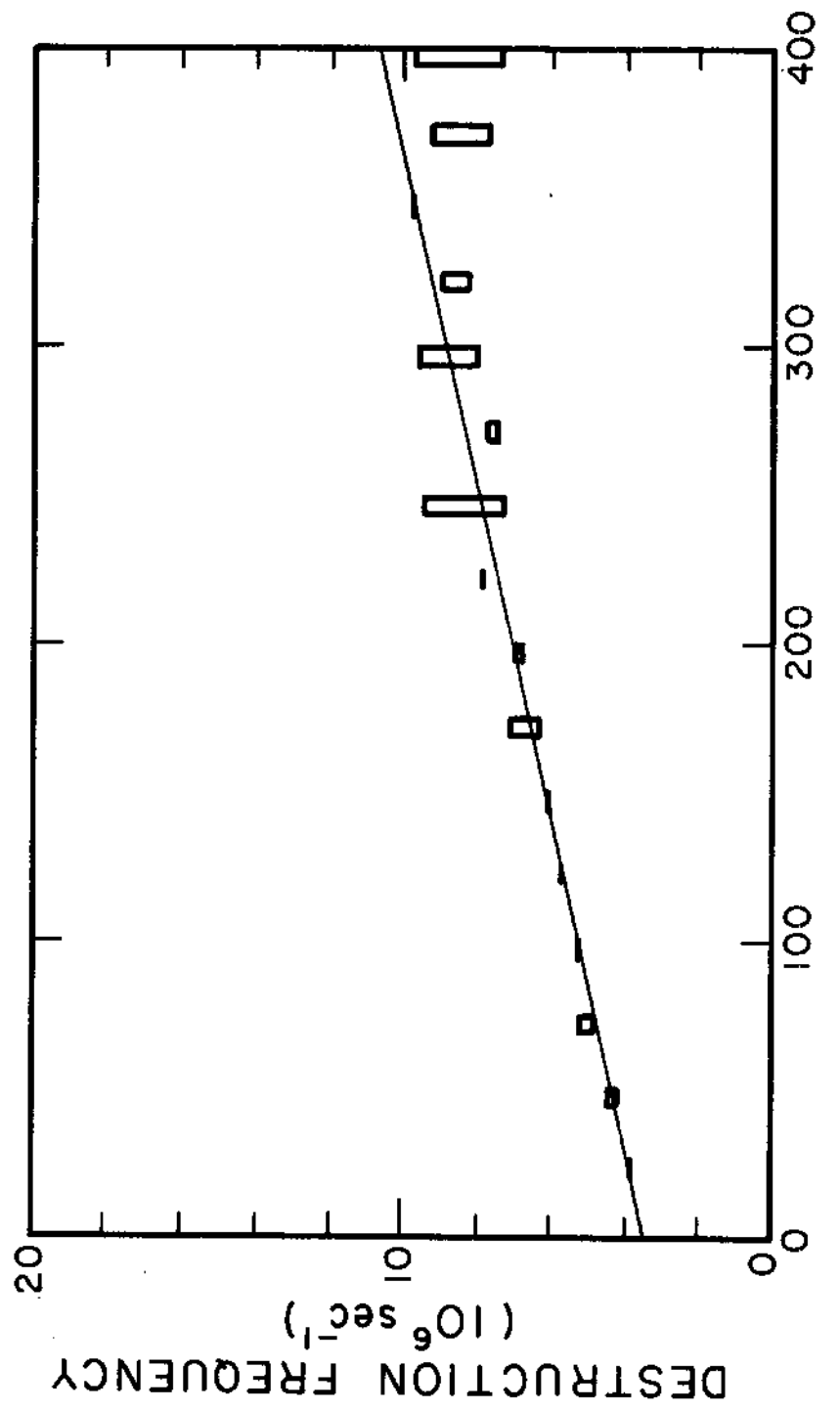

Fig. 30--Stern-Volmer plot of the destruction frequency of the exponential decay of the intensity at 4278 Å from the 50 μ of nitrogen used to monitor the He_2^+ concentration as a function of the partial pressure neon added to 770 torr of helium. The slope of the linear approximation corresponds to a rate coefficient of 5.5 x 10^{-10} cm^3/sec.

Fig. 31--Graphs as functions of helium pressure of the measured destruction frequencies of the transient intensities of 4278 Å radiation from the 50 μ Hg of nitrogen used to monitor the time dependence of the He_2^+ concentration. Partial pressures of the added CO reactant are indicated and comparison values of ν computed from Eq. (5.4) using previously reported bimolecular rate coefficients are shown together with the reported experimental uncertainty. Linear approximations are shown which best fit the data while remaining consistent with Eq. (5.5). The dashed line records base conditions of destruction frequency in the absence of the added reactant obtained from the 50 μ Hg nitrogen data of Fig. 24, and filled circles record agreement of subsequent remeasurements performed at the end of the data set shown. Open triangles plot supplementary data obtained from the intensity of the fluorescence from CO^+ product ions analyzed according to Eq. (5.8).

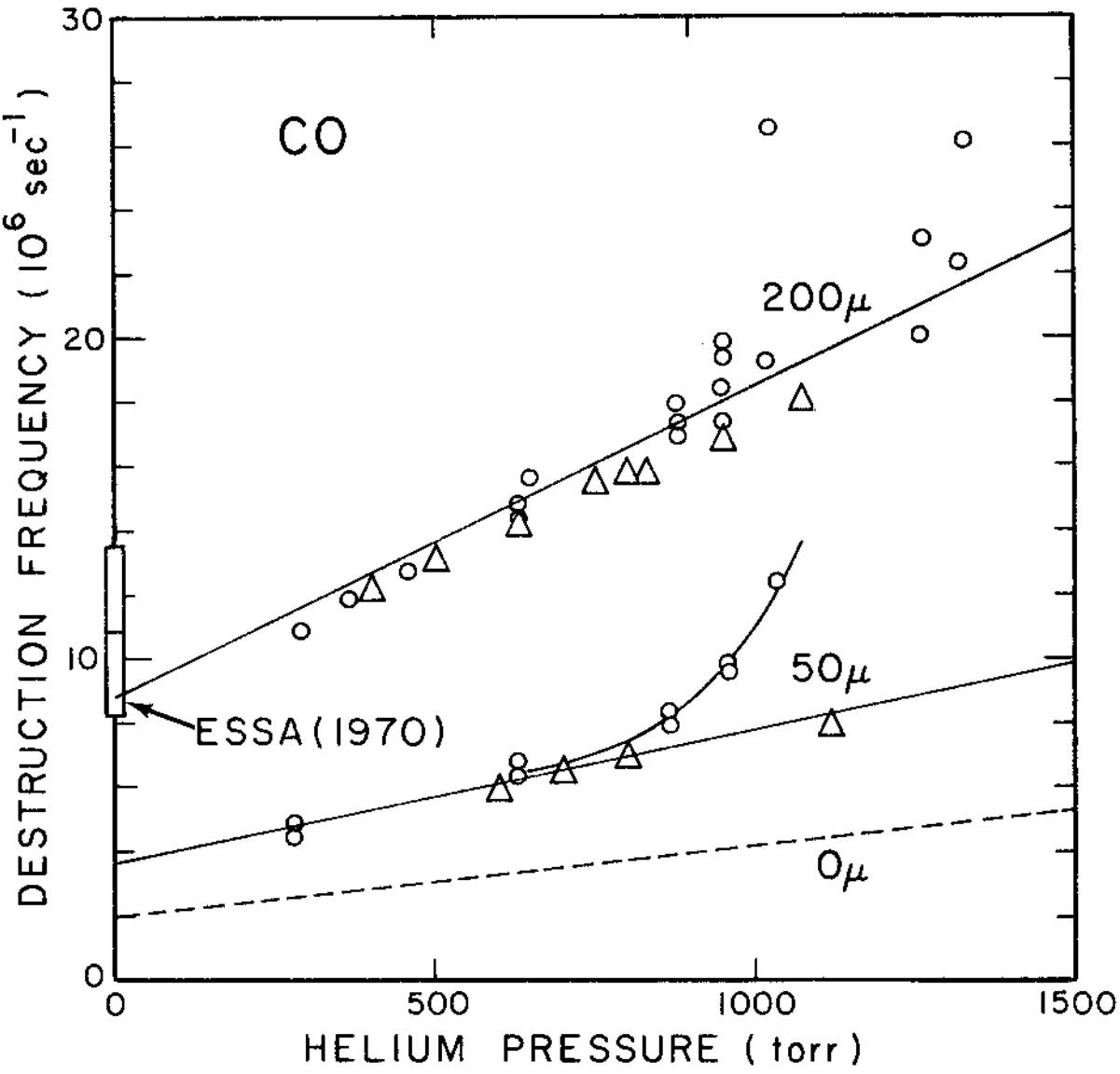
CO
200μ
50μ
0μ
ESSA (1970)
DESTRUCTION FREQUENCY (10^6 sec^{-1})
HELIUM PRESSURE (torr)
0
10
20
30
0
500
1000
1500

Fig. 32--Graphs as functions of helium pressure of the measured destruction frequencies of the transient intensities of 4278 Å radiation from the 50 μ Hg of nitrogen used to monitor the time dependence of the He_2^+ concentration. Partial pressures of the added CO_2 reactant are indicated and comparison values of ν computed from Eq. (5.4) using previously reported bimolecular rate coefficients are shown together with the reported experimental uncertainty. Linear approximations are shown which best fit the data while remaining consistent with Eq. (5.5). The dashed line records base conditions of destruction frequency in the absence of the added reactant obtained from the 50 μ Hg nitrogen data of Fig. 24, and filled circles record agreement of subsequent remeasurements performed at the end of the data set shown.

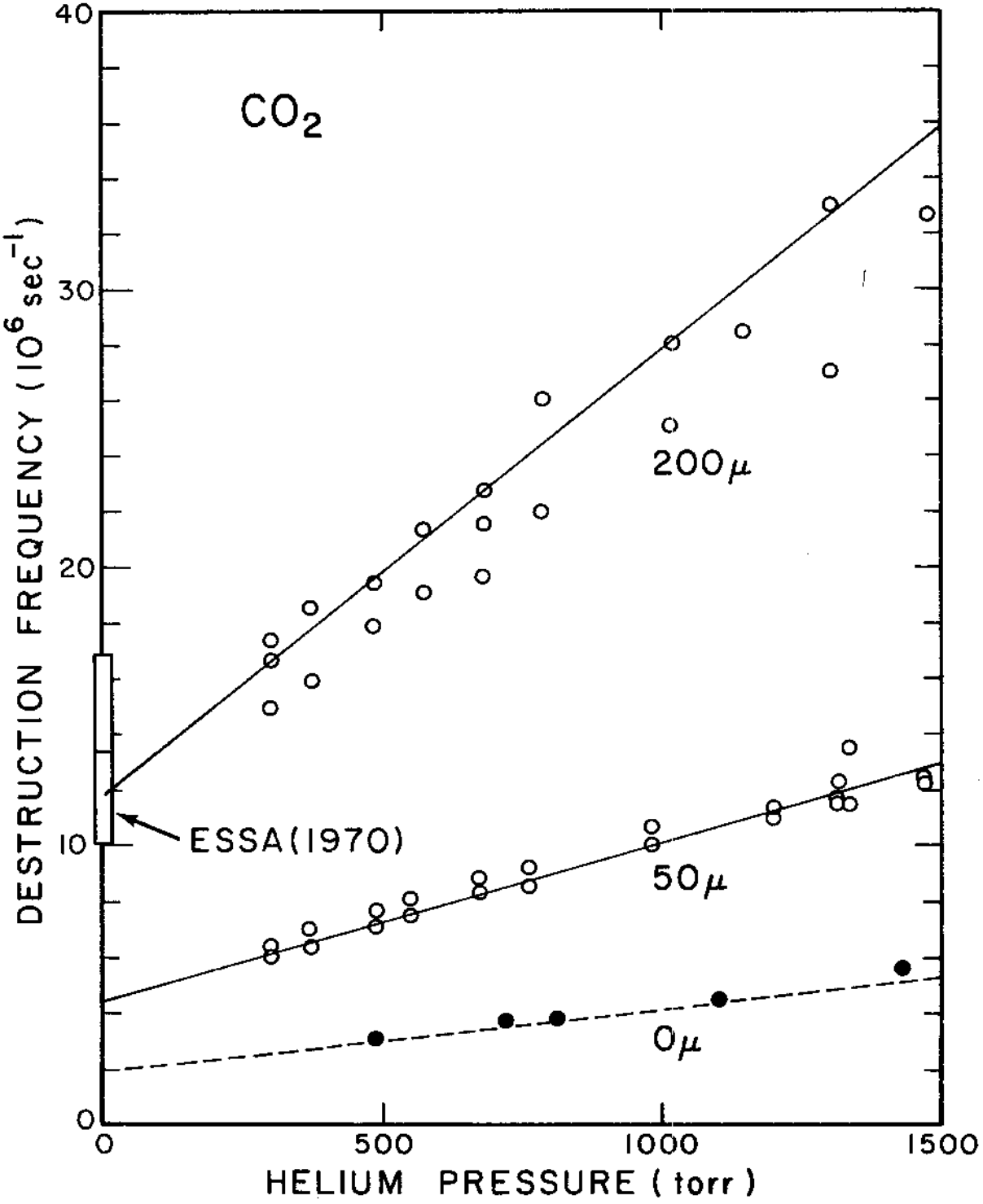
CO_2
200μ
50μ
0μ
ESSA(1970)
DESTRUCTION FREQUENCY (10^6 sec^{-1})
HELIUM PRESSURE (torr)
0
10
20
30
40
0
500
1000
1500

REFERENCES

[1]D. R. Bates and H. S. W. Massey, Proc. Roy. Soc. (London), A192, 1 (1947).

[2]E. W. McDaniel, V. Cermark, A. Dalgarno, E. E. Ferguson, and L. Friedman, Ion-Molecular Reactions (Wiley-Interscience, New York, 1970).

[3]H. J. Oskam, Doctoral Dissertation, University of Utrecht (1957); Philips Res. Rept. 13, 40 (1958).

[4]L. B. Loeb, J. Appl. Phys. 29, 1369 (1958).

[5]M. Pahl and U. Weimer, Naturwissenschaften 44, 484 (1957).

[6]H. J. Oskam and V. R. Mittelstadt, Phys. Rev. 132, 1435 (1963).

[7]C. B. Collins, W. W. Robertson, E. E. Ferguson, and F. A. Matsen, J. Am. Chem. Soc. 84, 676 (1962).

[8]C. B. Collins and W. W. Robertson, Spectrochemica Acta 19, 747 (1963).

[9]C. B. Collins and W. W. Robertson, J. Chem. Phys. 40, 701 (1964).

[10]F. C. Fehsenfeld, A. L. Schmeltekopf, P. D. Goldan, H. I. Schiff and E. E. Ferguson, J. Chem. Phys. 44, 4087 (1966).

[11]G. Gioumousis and D. P. Stevenson, J. Chem. Phys. 40, 860 (1964).

[12]D. B. Dunkin, F. C. Fehsenfeld, A. L. Schmeltekopf, and E. E. Ferguson, J. Chem. 49, 1365 (1968).

[13]D. K. Bohm, N. G. Adams, M. Mosesman, D. B. Dunkin, and E. E. Ferguson, J. Chem. Phys. 52, 5094 (1970).

[14]C. B. Collins, A. J. Cunningham, S. M. Curry, B. W. Johnson, and M. Stockton, Appl. Phys. Lett. 24, 477 (1974).

[15]C. B. Collins, A. J. Cunningham and M. Stockton, Appl. Phys. Lett. 25, 344 (1974).

[16]C. B. Collins and A. J. Cunningham, Appl. Phys. Lett. 27, 127 (1975).

[17]R. A. Waller, C. B. Collins, and A. J. Cunningham, Appl. Phys. Lett. 27, 323 (1975).

[18]G. H. Bearman, H. H. Harris and J. J. Leventhal, Appl. Phys. Lett. 28, 345 (1976).

[19]G. H. Bearman, J. D. Earl, R. J. Pieper, H. H. Harris, and J. J. Leventhal, Phys. Rev. A13, 1734 (1976).

[20]M. Bourène and J. LeCalvé, J. Phys. (Paris) 32, 29 (1971).

[21]W. Schottky, Phys. Z. 25, 635 (1924). For a refinement of Schottky's Analysis, see R. G. Fowler, Proc. Phys. Soc. (London) 80, 620 (1962).

[22]M. A. Biondi and S. C. Brown, Phys. Rev. 75, 1700 (1949).

[23]P. Langevin, Ann. Chim. Phys. 5, 245 (1905).

[24]D. K. Bohme, J. B. Hasted, and P. P. Ong, Chem. Phys. Lett. 1, 259 (1967).

[25]D. K. Bohme, J. B. Hasted, and P. P. Ong, J. Phys. B1, 879 (1968).

[26]J. F. Prince, C. B. Collins and W. W. Robertson, J. Chem. Phys. 40, 2619 (1964).

[27]J. B. Laudenslager, W. T. Huntress and M. T. Bowers, J. Chem. Phys. 61, 4600 (1974).

[28]H. F. Wellenstein, and W. W. Robertson, J. Chem. Phys. 56, 1077 (1972).

[29]C. B. Collins, B. W. Johnson, and M. J. Shaw, J. Chem. Phys. 57, 5310 (1972).

[30]A. V. Phelps and S. C. Brown, Phys. Rev. 86, 102 (1952).

[31]F. E. Niles and W. W. Robertson, J. Chem. Phys. 42, 3277 (1965).

[32]P. L. Paterson, J. Chem. Phys. 48, 3625 (1968).

[33]R. D. Poshusta, J. A. Haugen, and D. F. Zetik, J. Chem. Phys. 51, 3343 (1969).

[34]C. P. deVries and H. J. Oskam, Phys. Lett. 29A, 299 (1969).

[35]C. B. Collins, J. M. Carroll, F. W. Lee, and A. J. Cunningham, Appl. Phys. Lett. 28, 535 (1976).

[36]R. G. Gordon and Y. S. Kim, J. Chem. Phys. 56, 3122 (1972).

[37]G. Geotzel and N. Tralli, Some Mathematical Methods of Physics, (McGraw-Hill, Inc., New York, (1960), p. 21).

[38]R. Deloche, P. Monchicourt, M. Cheret, and F. Lambert, Phys. Rev. A13, 1140 (1976).

[39]D. C. Tyte and R. W. Nichols, Identification Atlas of Molecular Spectra, (University of W. Ontario, Dept. of Physics, Molecular Excitation Group, London, Ontario, 1965, p. 14).

[40]C. B. Collins, The Nitrogen Ion Laser, (Seventh Semi-Annual Technical Report, UTDP-ML-04 (1975)).

[41]D. Villarejo, R. R. Herm, and M. G. Inghram, J. Opt. Soc. Am. 56, 1574 (1966).